J. Am. Chem. Soc. **2001**, *123*, 7257−7270

7257

Investigation of the Mechanism of Alkane Reductive Elimination and Skeletal Isomerization in Tp′Rh(CNneopentyl)(R)H Complexes: The Role of Alkane Complexes

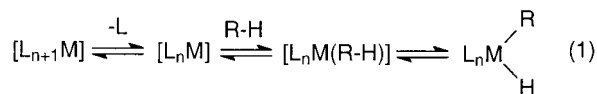**Todd O. Northcutt, Douglas D. Wick, Andrew J. Vetter, and William D. Jones***

Contribution from the Department of Chemistry, University of Rochester, Rochester, New York 14627

Received November 13, 2000

Abstract: Experiments are described that provide indirect evidence for the involvement of alkane σ-complexes in oxidative addition/reductive elimination reactions of Tp′Rh(L)(R)H complexes (Tp′ = tris-3,5-dimethylpyrazolylborate, L = CNCH$_2$CMe$_3$). Reductive elimination rates in benzene-d_6 were determined for loss of alkane from Tp′Rh(L)(R)H, where R = methyl, ethyl, propyl, butyl, pentyl, and hexyl, to generate RH and Tp′Rh(L)(C$_6$D$_5$)D. The isopropyl hydride complex Tp′Rh(L)(CHMe$_2$)H was found to rearrange to the *n*-propyl hydride complex Tp′Rh(L)(CH$_2$CH$_2$CH$_3$)H in an intramolecular reaction. The *sec*-butyl complex behaves similarly. These same reactions were studied by preparing the corresponding metal deuteride complexes, Tp′Rh-(L)(R)D, and the scrambling of the deuterium label into the α- and ω-positions of the alkyl group monitored by ^{2}H NMR spectroscopy. Inverse isotope effects observed in reductive elimination are shown to be the result of an inverse equilibrium isotope effect between the alkyl hydride(deuteride) complex and the σ-alkane complex. A kinetic model has been proposed using alkane complexes as intermediates and the selectivities available to these alkane complexes have been determined by kinetic modeling of the deuterium scrambling reactions.

Introduction

Numerous transition metal complexes are known to oxidatively add alkanes to form alkyl hydride complexes.[1] Alkane σ-complexes are increasingly implicated as significant intermediates along the reaction pathway toward oxidative addition (eq 1).[2] Direct study of the C−H bond insertion step by a

$$[L_{n+1}M] \underset{-L}{\rightleftharpoons} [L_nM] \underset{R-H}{\rightleftharpoons} [L_nM(R-H)] \rightleftharpoons L_nM\overset{R}{\underset{H}{\diagdown}} \quad (1)$$

coordinatively unsaturated transition-metal fragment has been examined using fast spectroscopic techniques in liquified or supercritical rare gases,[3] low-temperature gas matrices,[4] hydrocarbon solution,[5] and in the gas phase.[6]

Reductive elimination of alkane from an alkyl hydride complex is the microscopic reverse of oxidative addition of an alkane C−H bond to a coordinatively unsaturated metal center. Consequently, if formation of an alkane σ-complex precedes oxidative addition of a C−H bond, then this same σ-complex must also be an intermediate in the reductive elimination of an alkane from an alkyl hydride complex. The structures proposed for these alkane complexes include η^2-C,H, η^2-H,H, and η^3-H,H,H. Among the many pieces of evidence for the existence of alkane σ-complexes are the observations of hydrogen exchange between a metal deuteride complex and its alkyl ligands prior to reductive elimination,[7] the observation of inverse kinetic isotope effects,[8] and more recently, the direct observation of such complexes by TRIR and ^{1}H NMR spectroscopies.[9,10] Thermochemical studies also provide evidence for the interactions of alkanes with coordinatively unsaturated metals.[11]

η^2-C,H η^2-H,H η^3-H,H,H
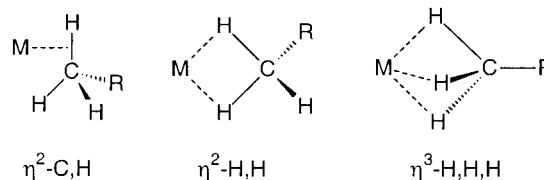
Norton and co-workers have shown that Cp$_2$W(D)(CH$_3$) and Cp$_2$W(H)(CD$_3$) exhibit intramolecular hydrogen exchange between the hydride and methyl ligands prior to methane reductive elimination.[7c] Mass spectroscopy of the reductive elimination

(1) (a) Janowicz, A. H.; Bergman, R. G. *J. Am. Chem. Soc.* **1982**, *104*, 352. (b) Hoyano, J. K.; Graham, W. A. G. *J. Am. Chem. Soc.* **1982**, *104*, 3723. (c) Janowicz, A. H.; Bergman, R. G. *J. Am. Chem. Soc.* **1983**, *105*, 3929. (d) Hoyano, J. K.; McMaster, A. D.; Graham, W. A. G. *J. Am. Chem. Soc.* **1983**, *105*, 7190. (e) Jones, W. D.; Feher, F. J. *Organometallics* **1983**, *2*, 562. (f) Seidler, P. F.; Wenzel, T. T.; Bergman, R. G. *J. Am. Chem. Soc.* **1985**, *107*, 4358. (g) Baker, M. V.; Field, L. S. *J. Am. Chem. Soc.* **1987**, *109*, 2825. (h) Ghosh, C. K.; Graham, W. A. G. *J. Am. Chem. Soc.* **1987**, *109*, 4726. (i) Hackett, M.; Whitesides, G. M. *J. Am. Chem. Soc.* **1988**, *110*, 1449. (j) Harper, T. G. P.; Shinomoto, R. S.; Deming, M. A.; Flood, T. C. *J. Am. Chem. Soc.* **1988**, *110*, 7915. (k) Belt, S. T.; Grevels, F. W.; Klotzbücher, W. E.; McCamley, A.; Perutz, R. N. *J. Am. Chem. Soc.* **1989**, *111*, 8373. (l) Kiel, W. A.; Ball, R. G.; Graham, W. A. G. *J. Organomet. Chem.* **1993**, *259*, 481. (m) Jones, W. D.; Hessell, E. T. *J. Am. Chem. Soc.* **1993**, *115*, 554. (n) Wick, D. D.; Goldberg, K. I. *J. Am. Chem. Soc.* **1997**, *117*, 110235.

(2) Hall, C.; Perutz, R. *Chem. Rev.* **1996**, *96*, 3125.

(3) (a) Schultz, R. H.; Bengali, A. A.; Tauber, M. J.; Weiller, B. H.; Wasserman, E. P.; Kyle, K. R.; Moore, C. B.; Bergman, R. G. *J. Am. Chem. Soc.* **1994**, *116*, 7369. (b) Bengali, A. A.; Schultz, R. H.; Moore, C. B.; Bergman, R. G. *J. Am. Chem. Soc.* **1994**, *116*, 9585.

(4) Haddleton, D. M.; McCamley, A.; Perutz, R. N. *J. Am. Chem. Soc.* **1988**, *110*, 1810.

(5) (a) Lian, T.; Bromberg, S. E.; Yang, H.; Proulx, G.; Bergman, R. G.; Harris, C. B. *J. Am. Chem. Soc.* **1996**, *118*, 3769. (b) Osman, R.; Pattison, D. I.; Perutz, R. N.; Bianchini, C.; Peruzzini, M. *J. Chem. Soc., Chem. Commun.* **1994**, 513. (c) Lees, A. J.; Purwoko, A. A. *Coord. Chem. Rev.* **1994**, *132*, 155.

(6) Wasserman, E. P.; Moore, C. B.; Bergman, R. G. *Science* **1992**, *255*, 315.

products from crossover experiments further support the intramolecular nature of the rearrangements. A number of other metal systems show similar exchanges in $M(CH_3)D$ compounds.[7] Girolami has recently observed *dynamic* exchange between the hydrogens of the methyl group and the hydride ligand in $(C_5Me_5)Os(dmpm)(CH_3)(H)^+$.[12]

Intramolecular rearrangement of an alkyl ligand has been observed by Periana and Bergman, in addition to hydrogen/deuterium exchange, in $Cp*Rh(PMe_3)(D)(^{13}CH_2CH_2)$ at low temperature.[7b] Migration of deuterium into the α position of the ethyl group occurs more rapidly than migration to the β position. Throughout the rearrangement the deuterium label remains attached to the ^{13}C-labeled carbon. Both migration processes are competitive with reductive elimination of $^{13}C,^2H$-ethane.

Direct evidence for alkane complexes first came from the study of photochemically generated $M(CO)_5$ (M = Cr, Mo, W) fragments in alkane and alkane/rare gas matrices.[13] George et al. also observed transient species by FTIR assigned as alkane complexes upon irradiation of $Cp*Re(CO)_3$ in hydrocarbon solvents.[9] Recently, low-temperature observation of the metal fragment $[CpRe(CO)_2]$ in cyclopentane by Ball and Geftakis provided direct spectroscopic evidence for the formation of an alkane complex,[10] although the data could not distinguish between a fluxional η^2-C,H and an η^2-H,H geometry for the complex.

Earlier studies of the [Tp′Rh(L)] fragment show it to be capable of activating a wide variety of alkane and arene C−H bonds (eq 2). In this report we will elucidate several of the key

$$\text{Tp'Rh(L)(PhN=L)} \xrightarrow[-\text{PhN=L}]{h\nu} \text{[Tp'Rh(L)]} \xrightarrow{\text{R-H}} \text{Tp'Rh(L)(R)(H)}$$

$$\text{L = CNCH}_2\text{CMe}_3 \qquad \qquad \text{R = Me, Et, } n\text{-Pr, } n\text{-pentyl, phenyl} \qquad (2)$$

mechanistic features of the interaction of the [Tp′Rh(L)] metal fragment with several alkanes (L = CNneopentyl, Tp′ = tris-(3,5-dimethylpyrazolyl)borate). Reductive elimination from linear alkyl hydride complexes is examined. Additionally, secondary alkyl hydride complexes are observed to rearrange intramolecularly to give the more stable linear *n*-alkyl hydride isomers. Kinetic isotope effects on both reductive elimination

and oxidative addition are measured, and determined to both be *normal* kinetic isotope effects ($k_H/k_D > 1$). All of these reactions are interpreted in terms of alkane σ-complexes as intermediates.

The mechanism by which the isomerizations occur can be broken down into several key steps: (1) C−H bond activation and its reverse, reductive elimination without dissociation of the alkane (these processes will be referred to herein more specifically as *reductive bond formation* and *oxidative bond cleavage*), (2) migration from one σ-alkane bond to another, and (3) dissociation of alkane from the alkane σ-complex. The relative rates of these processes, namely, dissociation vs oxidative bond cleavage of alkane (eq 3), migration vs oxidative bond cleavage (eq 4), and migration vs dissociation (eq 5), will

determine the observed product ratios. Kinetic simulations based on the results of isotopic labeling studies with several Tp′Rh-(L)(R)D complexes has allowed for the determination of the relative rates of each of these processes. Of particular relevance to these studies is the preliminary report by Flood on similar rearrangements of $[CnRh(L)RD]^+$ complexes (Cn = 1,4,7-triazacyclononane), which will be compared with the present results.[14]

Results and Discussion

Preparation of Tp′Rh(L)(R)H Complexes. Synthesis of a series of Tp′Rh(L)(R)Cl complexes (R = Me (**1-Cl**), Et (**2-Cl**), *n*-Pr (**3-Cl**), *n*-Bu (**4-Cl**), *n*-pentyl (**5-Cl**), *n*-hexyl (**6-Cl**), isopropyl (**3′-Cl**), and *sec*-butyl (**4′-Cl**); L = neopentylisocyanide)[15] is accomplished in reasonable yield (71%, **1-Cl** to 34%, **6-Cl**) by reaction of Tp′Rh(L)Cl_2 with the appropriate Grignard reagent.[16] Yields of the secondary alkyl chloride complexes are much lower than those obtained for linear alkyl complexes, 31% for **3′-Cl** and 13% for **4′-Cl**. The *sec*-butyl derivative **4′-Cl** is formed as a mixture of diastereomers in a 1:1 ratio and can be separated by fractional crystallization from methanol. All of these chloro derivatives have been fully characterized by ^1H NMR, ^{11}B NMR, ^{13}C NMR, and IR spectroscopies, as well as by elemental analysis, and are assigned as octahedral Rh^{III} complexes containing η^3 Tp′ ligands.[17] X-ray diffraction studies have been conducted on complexes **2-Cl** and **6-Cl**, confirming the structural conclusions made on the basis of spectroscopic data (see Supporting Information, Figures S-1 and S-2). Metrical parameters for the two structures show little difference in the

(7) (a) Buchanan, J. M.; Stryker, J. M.; Bergman, R. G. *J. Am. Chem. Soc.* **1986**, *108*, 1537. (b) Periana, R. A.; Bergman, R. G. *J. Am. Chem. Soc.* **1986**, *108*, 7332. (c) Bullock, R. M.; Headford, C. E. L.; Hennessy, K. M.; Kegley, S. E.; Norton, J. R. *J. Am. Chem. Soc.* **1989**, *111*, 3897. (d) Parkin, G.; Bercaw, J. E. *Organometallics* **1989**, *8*, 1172. (e) Gould, G. L.; Heinekey, D. M. *J. Am. Chem. Soc.* **1989**, *111*, 5502. (f) Stahl, S. S.; Labinger, J. A.; Bercaw, J. E. *J. Am. Chem. Soc.* **1996**, *118*, 5961. (g) Wang, C.; Ziller, J. W.; Flood, T. C. *J. Am. Chem. Soc.* **1995**, *117*, 1647. (h) Mobley, T. A.; Schade, C.; Bergman, R. G. *J. Am. Chem. Soc.* **1995**, *117*, 7822. (i) Chernaga, A.; Cook, J.; Green, M. L. H.; Labella, L.; Simpson, S. J.; Souter, J.; Stephens, A. H. H. *J. Chem. Soc., Dalton Trans.* **1997**, 3225.

(8) Examples of inverse k_H/k_D: (a) Cp*Ir(PMe_3)(H)(C_6H_{11}) in C_6D_6 at 130 °C, 0.7(1) (ref 7a). (b) Cp*Rh(PMe_3)(H)(C_2H_5) in toluene-d_8 at −30 °C, 0.5(1) (ref 7b). (c) Cp_2W(H)(CH_3) in CD_3CN at 72.6 °C, 0.75(4) (ref 7c). (d) Cp*_2W(H)(CH_3) in C_6D_6 at 100 °C, 0.77(7) (ref 7d). (e) [Cp_2Re-(H)(CH_3)][Cl] in CD_2Cl_2 at 9 °C, 0.8(1) (ref 7e). (f) [CnRh(PMe_3)(H)-(CH_3)][BAr_4] in C_6D_6 at 75 °C, 0.74(2) (ref 7g). (g) (tmeda)Pt(CH_3)(H)(Cl) in CH_3OH at −27 °C, 0.29 (ref 7f).

(9) By TRIR: Sun, X.-Z.; Grills, D. C.; Nikiforov, S. M.; Poliakoff, M.; George, M. W. *J. Am. Chem. Soc.* **1997**, *119*, 7521.

(10) By NMR: Geftakis, S.; Ball, E. *J. Am. Chem. Soc.* **1998**, *120*, 9953.

(11) (a) Brown, C. E.; Ishikawa, Y.; Hackett, P. A.; Rayner, D. M. *J. Am. Chem. Soc.* **1990**, *112*, 2530. (b) Klassen, J. K.; Selke, M.; Sorensen, A. A.; Yang, G. K. *J. Am. Chem. Soc.* **1990**, *112*, 1267. (c) Morse, J. M., Jr.; Parker, G. H.; Burkey, T. J. *Organometallics* **1989**, *8*, 2471.

(12) Gross, C. L.; Girolami, G. S. *J. Am. Chem. Soc.* **1998**, *120*, 6605.

(13) (a) Graham, M. A.; Perutz, R. N.; Poliakoff, M.; Turner, J. J. *J. Organomet. Chem.* **1972**, *34*, C34. (b) Perutz, R. N.; Turner, J. J. *J. Am. Chem. Soc.* **1975**, *97*, 4791.

(14) Flood, T. C.; Janak, K. E.; Iimura, M.; Zhen, H. *J. Am. Chem. Soc.* **2000**, *122*, 6783.

(15) In this manuscript, compound numbers refer to the length of the alkyl chain; primes denote 2-alkyl (iso- or sec-) isomers; greek letters (α, β, etc.) denote the location of deuterium relative along the chain relative to the metal.

(16) (a) Synthesis of **1-Cl**, **3-Cl**, and **6-Cl**: Wick, D. D.; Jones, W. D. *Inorg. Chem.* **1997**, *36*, 2723. (b) Synthesis of **5-Cl**: see ref 1m.

(17) Northcutt, T. O.; Lachicotte, R. J.; Jones, W. D. *Organometallics* **1998**, *14*, 5148.

Table 1. Summary of Kinetic Data for Reductive Elimination of RH from Tp′Rh(L)(R)H in C_6D_6 at 26 °C[a]

complex	k_{obs}, s^{-1}
Tp′Rh(L)(Me)H (**1**)	$4.51(3) \times 10^{-5}$
Tp′Rh(L)(Et)H (**2**)	$1.82(7) \times 10^{-4}$
Tp′Rh(L)(*n*-Pr)H (**3**)	$2.63(7) \times 10^{-4}$
Tp′Rh(L)(*n*-Bu)H (**4**)	$2.77(14) \times 10^{-4}$
Tp′Rh(L)(*n*-pentyl)H (**5**)	$2.70(8) \times 10^{-4}$
Tp′Rh(L)(*n*-hexyl)H (**6**)	$2.76(6) \times 10^{-4}$

[a] Errors are indicated in parentheses at the 95% confidence level (2σ).

coordination geometry at rhodium, including the Rh−Cα−Cβ angle of the alkyl group. Full structural details are included in the Supporting Information.

Complete conversion to the corresponding alkyl hydride complexes is effected by reaction of the alkyl chloride complexes with $[Cp_2ZrH_2]_2$ in benzene.[18] Conversion is generally rapid (e.g. $\tau_{1/2} \approx 200$ s for conversion of **3′-Cl** to Tp′Rh(L)-(*i*-Pr)H, **3′**). The hydride resonance for the primary alkyl hydride complexes **1−6** appears at ca. δ −14.9 ($J_{Rh-H} = 24.8$ Hz) while the hydride resonance for the two secondary alkyl hydride complexes, **3′** and **4′**, appears at δ −15.29 ($J_{Rh-H} = 25.2$ Hz) in C_6D_6 solvent.

Reductive Elimination of Primary Alkyl Hydrides in Benzene. Reductive elimination of alkane from the rhodium primary alkyl hydride complexes **1−6** in C_6D_6 was monitored by ¹H NMR spectroscopy at 26 °C. The reaction was found to be first order in metal complex, producing alkane and Tp′Rh-(L)(C₆D₅)D as the only products. No intermediates or isomers were detected. The rate of reductive elimination was determined for each complex by least-squares fit of the data to an exponential decay. The results are summarized in Table 1. Loss of methane from **1** is about 4× slower than loss of ethane from **2**, which is slightly slower (1.5×) than loss of alkane from the longer alkyl chain derivatives. The rate of alkane loss is identical from alkyl hydride complexes with a chain of three or more carbon atoms. An earlier study of **1** showed evidence for a minor bimolecular component to the displacement of methane by benzene.[18] Consequently, all experiments reported here were carried out in neat benzene solvent, so that the rate of formation of Tp′Rh(L)(C₆D₅)D would appear first order.

Isomerization of Secondary Alkyl Hydride Complexes. In benzene-d_6 solution at ambient temperature Tp′Rh(L)(*i*-Pr)H, **3′**, prepared from **3′-Cl** and $[Cp_2ZrH_2]_2$, is observed to rearrange over the course of an hour to give the *n*-propyl isomer, **3**. The secondary alkyl hydride complex is easily distinguished from the primary complex by virtue of the difference in chemical shift and coupling constant of the hydride ligand.[19] The isomerization of **3′** to **3** proceeds with a half-life of approximately 25 min. Competitive with isomerization is the reductive elimination of propane from **3′** to give Tp′Rh(L)-(C₆D₅)D. Loss of propane from **3** produced in situ must also be occurring at the same rate as that measured from the independently prepared *n*-propyl hydride, contributing to the appearance of Tp′Rh(L)(C₆D₅)D. The distribution of species is shown in Figure 1. An empirical fit of the kinetic model shown in Scheme 1 to the observed data required the presence of a direct pathway from **3′** to Tp′Rh(L)(C₆D₅)D as Tp′Rh(L)-(C₆D₅)D is formed more rapidly than **3**. Importantly, the rearrangement of **3′** to **3** must be occurring intramolecularly

(18) Wick, D. W.; Reynolds, K. A.; Jones, W. D. *J. Am. Chem. Soc.* **1999**, *121*, 3974.

(19) This phenomenon has been noted by others: Janowicz, A. H.; Bergman, R. G. *J. Am. Chem. Soc.* **1983**, *105*, 3929.
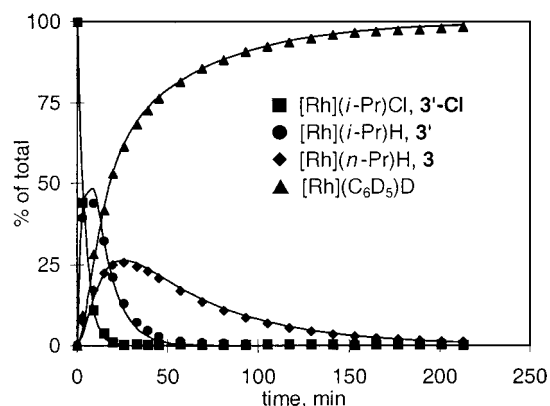
Figure 1. Distribution of species for the reaction of Tp′Rh(L)(*i*-Pr)-Cl, **3′-Cl**, with $[Cp_2Zr(H)_2]_2$ in C_6D_6 at 26 °C.

Scheme 1
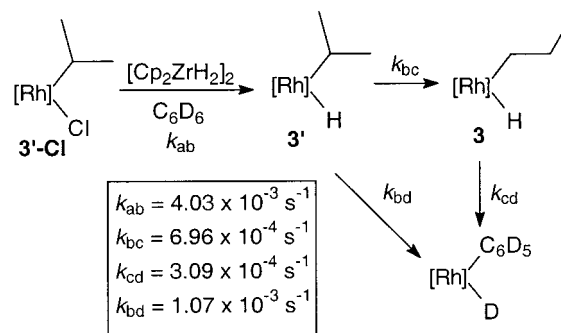
Scheme 2
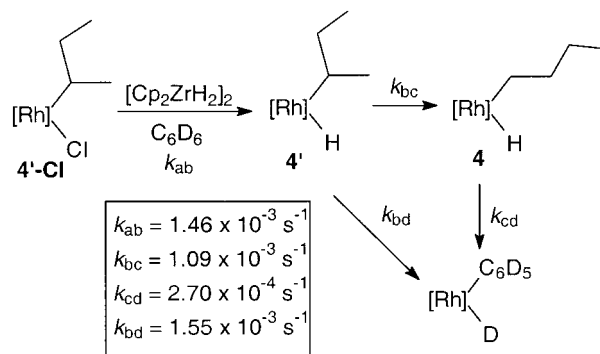
since C_6D_6 solvent would scavenge any [Tp′Rh(L)] produced by reductive elimination followed by dissociation of alkane.

The *sec*-butyl derivative shows similar behavior. Reaction of a 1:1 mixture of diastereomers of **4′-Cl** with $[Cp_2Zr(H)_2]_2$ affords a 1:1 mixture of diastereomers of **4′**. Both diastereomers are observed to decay at the same rate to afford the rearranged *n*-butyl hydride, **4**. Loss of butane from **4′** to give Tp′Rh(L)-(C₆D₅)D is competitive with the rearrangement process (Scheme 2). Identical rates are observed when the reaction is performed with a single diastereomer. Reaction of one diasteriomer of **4′-Cl** (isolated by crystallization) with $[Cp_2Zr(H)_2]_2$ gives only one diastereomer of **4′**, implying that the Cl/H exchange is stereospecific and that reversible reductive bond formation and oxidative bond cleavage of the β-C−H bonds is *not* occurring.

To further examine the nature of the rearrangement, the isotopically labeled isopropyl deuteride complex **3′-d_1** was prepared by use of $[Cp_2ZrD_2]_2$ as the hydride source in the reaction with **3′-Cl**. A doublet of 1:1:1 triplets (δ 0.832, $J_{HH} = 7.1$ Hz, $J_{HD} = 1.2$ Hz) is observed for the methyl groups in free propane produced during the reductive elimination of

Scheme 3. Reductive Bond Formation from **3′-d_1** Is Irreversible
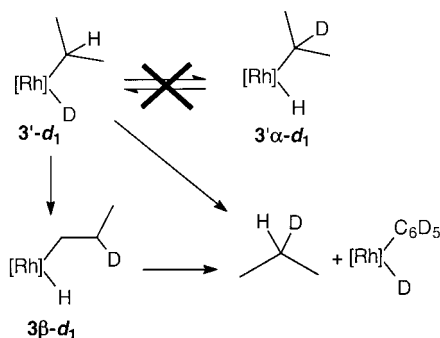
propane from **3′-d_1** (δ 0.848, J_{HH} = 7.2 Hz). The methylene resonance, a septet in fully protonated propane (δ 1.25), appears as a broad multiplet of low intensity. These results are consistent with the formation of CH_3CHDCH_3 in loss of propane from **3′-d_1**.

The isopropyl hydride isotopomer, Tp′Rh(L)(CD(CH$_3$)$_2$)H, was *not* observed, as might be expected for a reversible reductive bond formation/oxidative bond cleavage process at the β-carbon (Scheme 3). Furthermore, the deuterium label was observed only in the secondary positions in both **3β-d_1** and free propane-d_1 in the ^{2}H NMR spectrum of the reaction at intermediate times. The lack of isotopic scrambling into the α-position of **3′-d_1** implies that *rearrangement and/or dissociation are favored over activation of the secondary C−H bond, i.e., reductive bond formation in isopropyl hydride **3′** is irreversible.*

Similar observations are made with the *sec*-butyl deuteride derivative. Deuterium substitution in **4′-d_1** resulted in the appearance of label in *both* secondary positions in **4-d_1** produced in situ (eq 6). The concentration of the label is slightly higher in the β position (17% **4β-d_1**) than in the γ position (14% **4γ-d_1**) as observed by ^{2}H NMR spectroscopy. (See Supporting Information.)
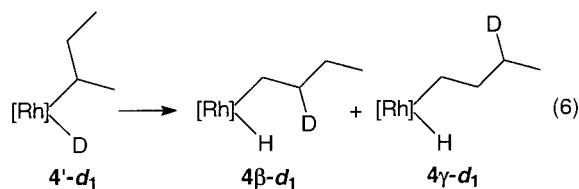
The selectivity of the [Tp′Rh(L)] fragment for activation of primary C−H bonds over secondary C−H bonds in normal alkanes has been previously reported.[1m] Conclusions regarding the kinetic vs thermodynamic origins of this selectivity remained uncertain in this earlier work. Since only primary alkyl hydride products were observed, it could be possible that secondary C−H activation occurred initially but that these kinetically formed species rearranged rapidly under the reaction conditions to the thermodynamically preferred primary derivatives. The present experiments show, however, that the lifetime of the isopropyl hydride is sufficiently long that detection of **3′** under the conditions employed in the low-temperature photochemical activation of propane by Tp′Rh(L)(η^2-PhN=C=NCH$_2$C(CH$_3$)$_3$), **7**, would have been possible were it present within the reaction. Given the lack of secondary C−H bond activation in the earlier alkane activation experiments and the observed rearrangement of **3′** to **3**, it can be concluded that *the activation of the primary C−H bonds by [Tp′Rh(L)] is both kinetic and thermodynamic in nature.*

Measurement of Kinetic Isotope Effects. Use of [Cp$_2$Zr-(D)$_2$]$_2$ in place of [Cp$_2$Zr(H)$_2$]$_2$ allows for the formation of the deuteride isotopomers, **1−4′-d_1**. As mentioned above, for complexes **3′-d_1** and **4′-d_1** the deuterium label is observed only in the secondary position of the alkane upon reductive elimination. No scrambling of the label into primary sites is observed. No secondary hydrides were observed by ^{1}H NMR spectroscopy during the rearrangement and elimination of alkane-d_1 from **3′-d_1** and **4′-d_1**, consistent with an irreversible reductive bond formation process. These latter observations allow for the measurement of a kinetic isotope effect for the fundamental step involving reductive bond formation to generate an alkane σ-complex (eq 7), which corresponds to the ratio of the observed
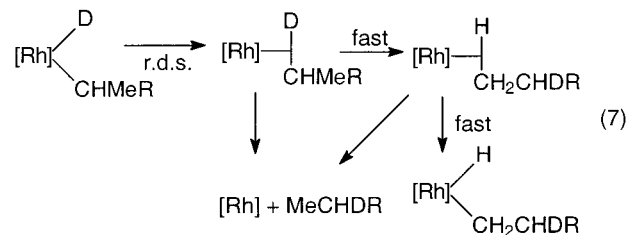
rate constants $(k_{bc} + k_{bd})_H/(k_{bc} + k_{bd})_D$ in Schemes 1 and 2, since re-addition to a secondary C−H bond is slow relative to migration and insertion into a terminal C−H bond or dissociation. For **3′-d_1** the measured isotope effect (k_H/k_D) was 2.1, a *normal* isotope effect. For **4′-d_1** a similar value was obtained (k_H/k_D = 2.7).

The isotope effect on the reverse reaction, oxidative bond cleavage of a C−H bond in an alkane complex, has also been determined. Photolysis of Tp′Rh(L)(η^2-PhN=C=NCH$_2$−C(CH$_3$)$_3$), **7**, at 5 °C in C$_6$F$_6$ in the presence of CH$_2$D$_2$ leads to the formation of a mixture of C−H and C−D activated products, presumably via a methane σ-complex (eq 8). ^{1}H{^{2}H} NMR
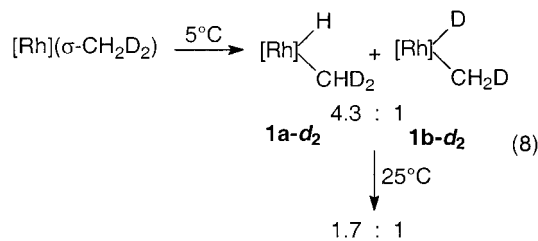
analysis at 9 °C at early reaction times reveals a 4.3:1 mixture of Tp′Rh(L)(CHD$_2$)H, **1a-d_2**, and Tp′Rh(L)(CH$_2$D)D, **1b-d_2**. Assuming that the σ-CH$_2$D$_2$ complex has equal access to the C−H and C−D bonds (vide infra),[20] this ratio reflects the kinetic isotope effect on oxidative bond cleavage in an alkane complex, which is again observed to be a *normal* kinetic isotope effect. Upon standing at room temperature, this mixture equilibrates to yield a 1.7:1 ratio of **1a-d_2** and **1b-d_2**. A more thorough, quantitative treatment of H/D scrambling will be given in a subsequent section.

Alkane σ-complexes are increasingly implicated as significant intermediates in C−H bond activation, and the observation of

---

(20) In the σ-cyclopentane complex described by Ball, the metal was believed to rapidly migrate from one C−H to the other within the same methylene unit, although an η^2-H,H binding geometry could not be ruled out. In studies of an agostic methyl group by Shapley in Os$_3$(CH$_2$D)(CO)$_{11}$, migration between C−H and C−D was fast on the NMR time scale and a preference for binding C−H vs C−D was only 1.25 (see ref 27). In the present system, a similar slight preference for binding C−H vs C−D bonds may be present, although studies of [Cp*Rh(CO)] in liquid krypton show a distinct preference for binding C−D bonds over C−H bonds (see ref 3).

an inverse kinetic isotope effect for reductive elimination from metal alkyl hydride complexes is commonly cited as providing evidence for these species.[8] These inverse isotope effects are often explained by the presence of a preequilibrium involving an alkane σ-complex followed by a rate-determining alkane dissociation step with the observed isotope effect being the product of the equilibrium isotope effect and the kinetic isotope effect, $K \cdot k$ (eq 9). Inverse isotope effects, however, can also be accommodated by single-step mechanisms provided the transition state is sufficiently late (i.e., a very product-like transition state).[21]

$$L_nM \underset{R}{\overset{H}{\big\langle}} \underset{K}{\rightleftharpoons} [L_nM(R-H)] \xrightarrow{k} [L_nM] \quad (9)$$
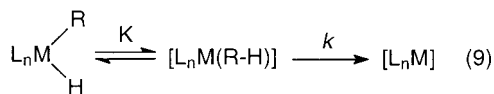
Normal kinetic isotope effects were observed for the reductive elimination of alkane from **3′** and **4′**. Additionally, no H/D exchange at the secondary position was observed over the course of the reaction. These observations are consistent with the trend noted by Bercaw and Labinger, in which only complexes exhibiting H/D scrambling showed inverse isotope effects.[7f] The lack of scrambling in secondary alkyl deuteride complexes allows the isotope effect on reductive bond formation from a secondary alkyl hydride to be unambiguously assigned.

The C−H/D bond activation of CH_2D_2 by **7** is, to the best of our knowledge, the first direct measurement of an internally competitive kinetic isotope effect on the oxidative bond cleavage of a σ-complexed alkane by a transition metal complex. The use of an inert solvent, C_6F_6, precludes side reactions with solvent. Photolysis and spectroscopy at low temperature place the reaction under kinetic control, i.e., no rearrangement of the initially formed bond activation products occurs. Statistically, C−H and C−D bond activation are equally likely in CH_2D_2, making the observed product ratio a direct reflection of the isotope effect for oxidative bond cleavage of the σ-complexed methane. The value obtained, 4.3, is normal and larger than the isotope effect observed on reductive bond formation from **3′** and **4′**. Any H/D scrambling occurring before acquisition of the first $^1H\{^2H\}$ NMR spectrum would serve only to *decrease* the observed product ratio, making 4.3 a minimum value for the isotope effect on oxidative bond cleavage. If we assume that the isotope effect on reductive bond formation to generate an alkane complex is similar for different alkanes then these two *kinetic* isotope effects can be combined to give an equilibrium isotope effect of ~ 0.5 for the preequilibrium (K) prior to alkane dissociation in eq 9. This inverse value is similar to that seen for the overall loss of alkane from $Tp'Rh(L)(CD_3)D$ vs $Tp'Rh(L)(CH_3)(H)$, where $k_H/k_D = 0.62$.[18]

Also of relevance is the direct measurement of isotope effects on C−H vs C−D oxidative bond cleavage of cyclohexane and neopentane by $[Cp*Rh(CO)]$. In these fast IR studies, direct kinetic evidence was obtained for normal isotope effects on oxidative bond cleavage ($k_H/k_D = 4.4$ at 25 °C),[3] almost exactly what is seen in the present case using CH_2D_2.

Scrambling and Migration in Primary Alkyl Deuteride Complexes. The isotopic scrambling of **1-d_1** to **6-d_1** were monitored by $^2H\{^1H\}$ NMR spectroscopy at 26 °C. As described in a previous paper, $Tp'Rh(L)(CH_3)D$, **1-d_1**, scrambles with $Tp'Rh(L)(CH_2D)H$, **1α-d_1**, at a rate competitive with loss of CH_3D (see below).[18] For the other alkyl derivatives, two processes were generally observed to be competitive with alkane

(21) Cheng, T.-Y.; Bullock, R. M. *J. Am. Chem. Soc.* **1999**, *121*, 3150−3155.
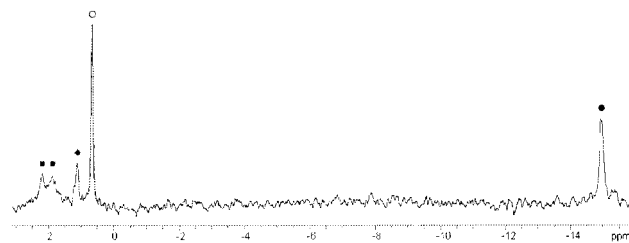
Figure 2. Sample $^2H\{^1H\}$ NMR spectrum of the rearrangement of $Tp'Rh(L)(CH_2CH_2CH_3)D$ (**3-d_1**, ●) to $Tp'Rh(L)(CDHCH_2CH_3)H$ (**3α-d_1**, ■, 2 diastereomers) and $Tp'Rh(L)(CH_2CH_2CDH_2)H$ (**3γ-d_1**, ◆) in C_6H_6. Free propane-d_1 (○) appears at δ 0.67.

loss: (1) scrambling of deuterium onto the α-carbon and (2) scrambling of deuterium into the terminal methyl group of the *n*-alkyl chain. The label was observed in both the α- and β-positions with ethyl complex **2-d_1**. The α-scrambled product, **2α-d_1**, grew to a maximum of 23% of all observable $Tp'Rh(L)$ species, while the β-migratory product, **2β-d_1**, grew to a maximum of ~ 16% over 450 min (eq 10). Similar reactivity was observed by Bergman in the doubly labeled complex $Cp*Rh(PMe_3)(*CH_2CH_3)D$ although relative amounts were not quantified.[7b]

$$Tp'(L)Rh(CH_2CH_3)D \rightleftharpoons Tp'(L)Rh(CDHCH_3)H$$
$$\textbf{2-}d_1 \qquad\qquad \textbf{2}\alpha\textbf{-}d_1 \qquad (10)$$
$$+ \ Tp'(L)Rh(CH_2CDH_2)H$$
$$\textbf{2}\beta\textbf{-}d_1$$
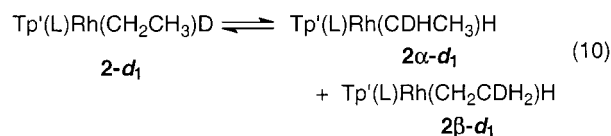
Complexes **3-d_1** to **6-d_1** exhibit similar behavior as monitored by $^2H\{^1H\}$ NMR spectroscopy (Figure 2), with α-scrambled products growing to a maximum of 18−23% of the observable species. As mentioned above, incorporation of the deuterium label into the *terminal methyl group* of the alkyl ligand was also observed. The amount of the terminally labeled species decreased as the chain length of the alkyl ligand increased, with ~ 8% of the label observed at the terminal methyl group in **3γ-d_1** to a minimum of ~ 4% observed in **5ϵ-d_1**. The methyl resonance of free hexane-d_1 obscured the small amount of label present in the methyl group of **6ϕ-d_1**, so that the amount of scrambled product could not be quantified. No other intermediates were observed during the course of the reaction.

Detailed Mechanism of Isomerization and Scrambling. The isomerization and scrambling processes observed in the $Tp'Rh$ alkyl hydride system can be accommodated by several different reaction mechanisms. However, the intramolecular nature of the reactions as well as the selectivity of the activation and isomerization process allow several of these possibilities to be discounted. Previous work by Bergman[7a] and Flood[14] has shown that the intramolecular rearrangement of alkyl hydride complexes does not take place via a reversible β-hydride elimination/insertion pathway. The observation of retention of deuterium-labeling with the appropriate carbon in the present studies also argues against this pathway. A mechanism in which the terminal methyl group of a straight-chained alkyl ligand is activated to give a metallocyclic complex that then eliminates to give an isomerized *n*-alkyl complex can be ruled out for several reasons. With increasing chain length, which might be expected to make the metallocycle more stable and thus lead to increased appearance of the label at the terminus, migration of the label monotonically decreases. Also, the Rh^V species
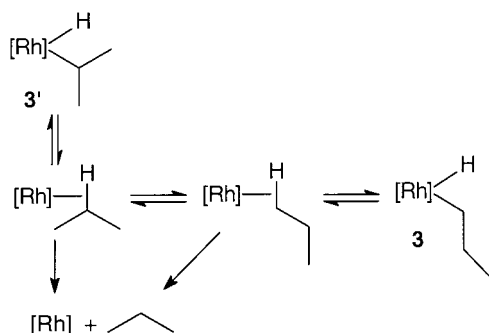
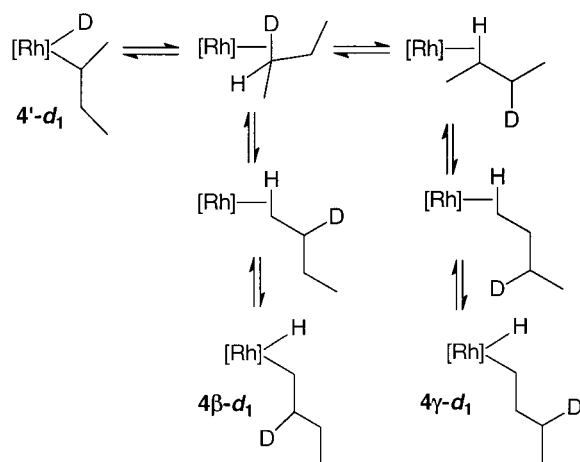**Scheme 4**

Scheme 5

Scheme 6
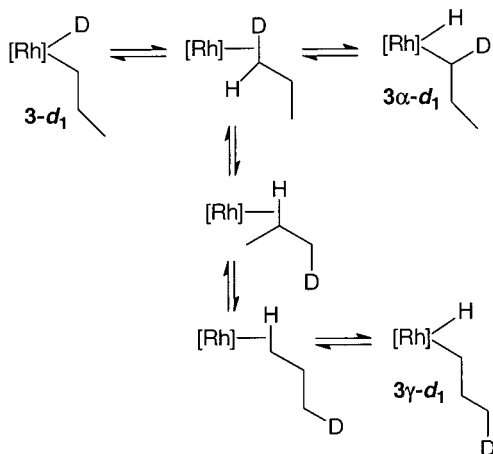
generated as an intermediate in such a mechanism would necessitate an η^3 or η^1 Tp′ ligand.[22]

Most consistent with the observed data is the presence of alkane complexes as intermediates in the isomerization and migration processes. The earlier flash studies by Bergman and Harris with Tp′Rh(CO)$_2$ provided direct evidence for the intermediacy of such a species.[5a] Once such an alkane complex is formed, the relative rates of migration, insertion into a C−H bond, and dissociation will control the observed product ratios. This detailed mechanistic sequence can be applied to the present studies.

Reductive bond formation from a secondary alkyl hydride complex such as isopropyl hydride **3′** generates a secondary σ-alkane complex. Migration to a primary C−H bond followed by oxidative bond cleavage of the primary C−H bond, and dissociation of the alkane to generate the 16e$^-$ fragment which activates C$_6$D$_6$ solvent, are competitive processes, as observed by growth of the *n*-propyl hydride **3** and Tp′Rh(L)(C$_6$D$_5$)D (Scheme 4). Lack of insertion into a secondary C−H bond implies that the barrier for a secondary C−H bond activation must be higher than that for alkane dissociation and/or migration from a secondary position to a primary position in an alkane σ-complex.

σ-Alkane complexes also account for the scrambling of deuterium label into the α- and terminal-methyl positions in the normal alkyl deuteride complexes such as **3-d_1** (Scheme 5). The intermediacy of alkane complexes also explains the decrease in label migration to the terminal end of linear alkyl hydride complexes with increasing chain length. With each additional methylene unit the percent migration decreases as there are more

(22) η^1 Tp ligands are extremely rare. For an example with Rh see: Paneque, M.; Sirol, S.; Trujillo, M.; Gutierrez-Puebla, E.; Monge, A.; Carmona, E. *Angew. Chem., Int. Ed.* **2000**, *39*, 218.

opportunities for dissociation of alkane as the metal center migrates down the alkyl chain. The amount of scrambling of the deuterium label into the α position, however, is nearly the same for all linear alkyl hydride complexes with alkyl groups with 2 or more carbons ($\sim$20%). A similar primary σ-alkane complex is involved in the α-scrambling process in each of these, and consequently, the extent of α-scrambling is nearly identical in all of the alkyl deuteride complexes.

Appearance of the label in the terminal methyl group of the longer chain alkanes (i.e. butyl or pentyl) requires migration from secondary-to-secondary C−H bonds in σ-alkane complexes. Secondary-to-secondary migration is also observed in the rearrangement of *sec*-butyl complex **4′-d_1**. The deuterium label appears in both secondary positions (β and γ) of the *n*-butyl complex that is formed (Scheme 6), indicating that migration occurs to each end of the chain. Appearance of the label in the δ-position during the scrambling of *n*-butyl deuteride complex **4-d_1** also necessitates migration from secondary-to-secondary C−H bonds.

One additional feature present in these systems needs to be addressed, namely, the hapticity of the Tp′ ligand during these reactions. Earlier studies by Bergman and Jones suggest that the Rh^I species commonly contain an η^2-Tp′ ligand whereas the Rh^{III} species have an η^3-Tp′ ligand. Ultrafast studies of Tp′Rh(CO)$_2$ by Bergman show direct evidence for such an η^3- to η^2-Tp′ conversion, and the rate is extremely fast ($\tau = 200$ ps).[5a] Such interconversions, if they occur in the present system, are also likely to be rapid and reversible and therefore do not have to be specifically included in a kinetic model of the mechanism. It should be kept in mind, however, that any hapticity changing equilibria are included in the rate constants that are obtained.

Kinetic Simulation of Alkane Migration: Methane. The detailed mechanism for the scrambling of the deuterium label into the methyl group of **1-d_1** is presented in Scheme 7. Five intrinsic rate constants govern the process, with the relative rates controlling the observed product ratios. With only three observable species in the present study (**1-d_1**, **1α-d_1**, and methane-d_1), an exact solution for all of the rate constants is not possible. Several assumptions may be made, however, which simplify the scheme and render the problem solvable: (1) all C−H bonds at a given carbon are accessed equally[20] and that exchange between η^2-C,H coordination at a given carbon of a σ-alkane complex is sufficiently rapid that it is kinetically unimportant, (2) the isotope effect on reductive bond formation to generate a σ-alkane complex is the same for all alkyl hydrides ($k_H^{RE}/k_D^{RE} = 2.1$), and (3) the rate constant for oxidative bond

Tp′Rh(CNneopentyl)(R)H Complexes)

J. Am. Chem. Soc., Vol. 123, No. 30, 2001 7263
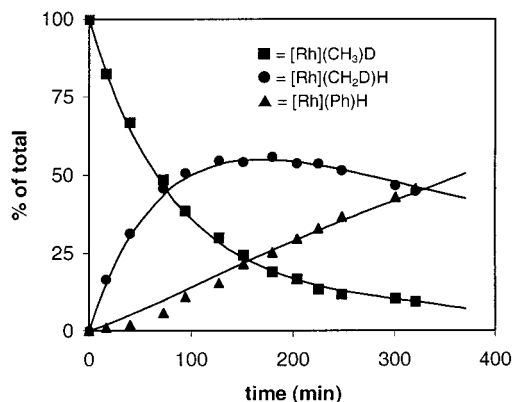
Figure 3. Distribution of species for the rearrangement of **1-d_1** in C$_6$D$_6$ at 26 °C. Symbols represent observed data. Solid lines represent simulated data.

Table 2. Summary of Simulated Rate Constants for Isotopic Scrambling of **1-d_1** in C$_6$D$_6$ at 26 °C[a]

rate constant	k, s^{-1}
k_{RE}^H	4.18 (9) × 10^{-4}
k_{RE}^D	**1.99 (4) × 10^{-4}**
k_{OA}^H	2.15 × 10^6
k_{OA}^D	**4.3 (4) × 10^5**
k_d	**8.0 (2) × 10^5**

[a] Rate constants that were allowed to vary independently are indicated in bold. Errors are indicated in parentheses at the 95% confidence level (2σ).

cleavage to a C–H bond in an alkane complex is similar to that observed by Bergman and Harris in their study of oxidative addition by the [Tp′Rh(CO)] fragment ($k_{OA}^H = 2.15 \times 10^6$ s^{-1}).[5a] It will be shown that this latter assumption is necessary to numerically simulate the observed data, but that the actual *value* assumed for this rate constant is irrelevant to the *selectivities* available to the σ-alkane complex.

Simulations were carried out using Frieden's KINSIM/FITSIM program, which incorporates Gear's method for the solution of "stiff" differential equations and permits optimization of rate constants for a given mechanism.[23] Figure 3 shows the agreement between the observed and simulated results for **1-d_1**. Summarized in Table 2 are the results of the kinetic simulation performed using the assumptions presented above. While the *absolute* values of the fast rate constants are dependent upon the value used in assumption 3 above, the *relative* values remain unchanged when k_{OA}^H was varied over 6 orders of magnitude. The free energy diagram for the oxidative addition of CH$_3$D by [Tp′RhL] is presented in Figure 4. In this diagram, x represents the assumed barrier for oxidative bond cleavage of a C–H bond in an alkane complex, k_{OA}^H, and cannot be determined from the current experiments. In essence, the free energy of the (n^2-CH$_3$D) σ-complex cannot be determined. The value for k_{OA}^H measured by Bergman and Harris, 2.15×10^6 s^{-1}, corresponds to a value for x of 8.2 kcal/mol. The simulation provides the relative rates for the processes available to the methane σ-complex. The relative rates of C–H oxidative bond cleavage to dissociation to C–D oxidative bond cleavage are 15:2:1, and include the statistical factors appropriate for CH$_3$D. For CH$_4$ itself, the rate of oxidative bond cleavage to dissociation can be predicted to be 11:1 ($4k_{OA}^H/k_d$).

The barrier to dissociation of methane to generate [Tp′Rh-(L)] from the methane σ-complex of 9.4 kcal/mol (1.2 + x) is

(23) Prof. Carl Frieden, Department of Biological Chemistry, Box 8231, Washington University School of Medicine, St. Louis, MO 63110. Available on the web; search KINSIM.
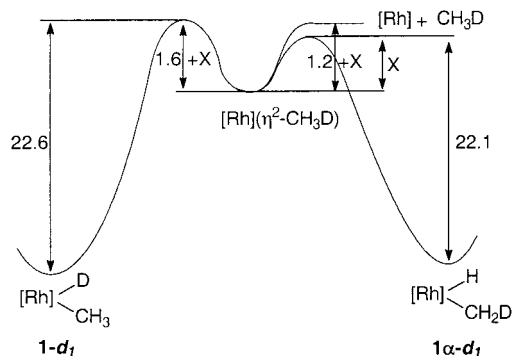
Figure 4. Free energy diagram for the activation of CH$_3$D by [Tp′Rh-(CNR)].

Scheme 7
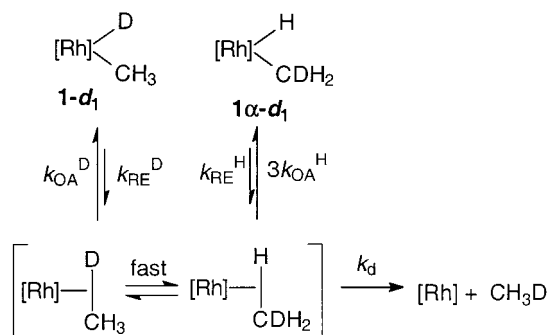
Scheme 8
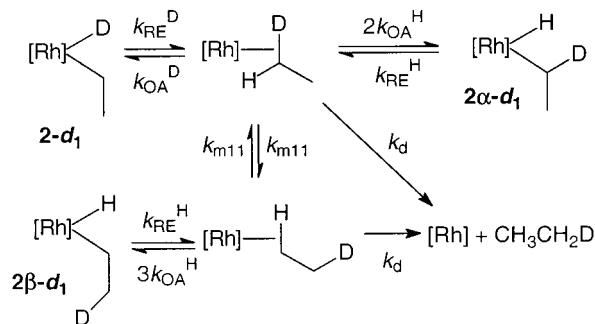
in good agreement with previous estimates of the strength of the alkane–metal interaction (~10 kcal/mol), established in studies of photochemically generated metal fragments in alkane/rare gas matrices.[11c] The value for K_{eq} obtained for the observed equilibration of **1-d_1** and **1α-d_1** based on the results of the simulation is 7.1, in good agreement with the observed value of 6.3 near the end of the experiment.[18] The value for the kinetic isotope effect on oxidative bond cleavage (k_{OA}^H/k_{OA}^D) obtained from the simulated values is 5.0, only slightly higher than the isotope effect measured in the photochemical oxidative addition of CH$_2$D$_2$ by **7** of 4.3. The good agreement of the simulated values with the directly measured values provides support for the validity of the assumptions concerning isotope effects made in the simulation model.

Kinetic Simulation of Alkane Migration: Ethane. Similar treatment of scrambling and migration data for ethyl deuteride complex **2-d_1** yields rates of oxidative bond cleavage, reductive bond formation, and dissociation as well as the rate of primary-to-primary migration (Scheme 8). The value for the rate constant for oxidative bond cleavage of C–D bonds (k_{OA}^D) obtained in the simulation of scrambling in **1-d_1** was used for simulation of **2-d_1** and held constant (i.e., the isotope effect for oxidative bond cleavage was maintained at $k_{OA}^H/k_{OA}^D = 4.97$). With **2-d_1**,

Figure 5. Distribution of species for the rearrangement of **2-d_1** in C_6H_6 at 26 °C. Symbols represent observed data. Solid lines represent simulated data.
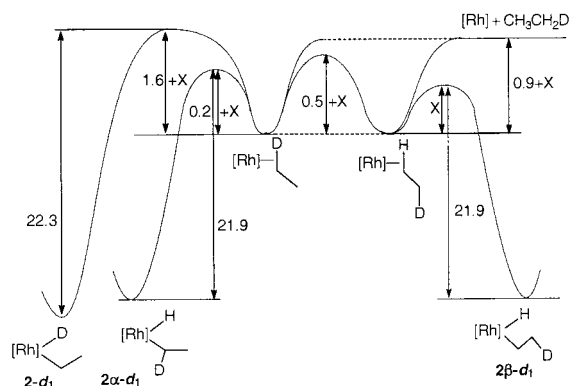
Figure 6. Free energy diagram for the activation of CH_3CH_2D by [Tp′Rh(CNR)].

Table 3. Summary of Simulated Rate Constants for Isotopic Scrambling of **2-d_1** in C_6D_6 at 26 °C[a]

rate constant	k, s^{-1}
k_{RE}^H	6.58 (9) × 10^{-4}
k_{RE}^D	**3.13 (9) × 10^{-4}**
k_{OA}^H	2.15 × 10^6
k_{OA}^D	4.33 × 10^5
k_{m11}	**3.0 (5) × 10^6**
k_d	**1.55 (9) × 10^6**

[a] Rate constants that were allowed to vary independently are indicated in bold. Errors are indicated in parentheses at the 95% confidence level (2σ).

an additional rate constant appears for migration of the metal from the primary C−H bond on one methyl group to the other (k_{m11}). The comparison of simulated and observed data is shown in Figure 5, and rate constants are summarized in Table 3 and presented as a free energy diagram in Figure 6.

Relative rates of oxidative bond cleavage, migration, and dissociation of C_2H_5D are as follows: $2k_{OA}^H > k_{m11} > k_d > k_{OA}^D$ (10:7:4:1). Oxidative bond cleavage of a C−D bond is the slowest process involved, as was the case for scrambling in **1-d_1**. Like methane, oxidative bond cleavage of a methyl C−H bond in C_2H_6 is faster than ethane dissociation but only by a factor of 4 instead of 11 ($\Delta\Delta G^{\ddagger}$ is only 0.9 kcal/mol). Consequently only ∼23% α-scrambling is seen prior to ethane loss compared with ∼50% in methane. Migration from primary C−H bond to primary C−H bond occurs at approximately twice the rate of dissociation. The effects of the relative rates on product ratios are easily identifiable in the distribution of species plots, with much less of the α-scrambled product (∼23%)

Scheme 9
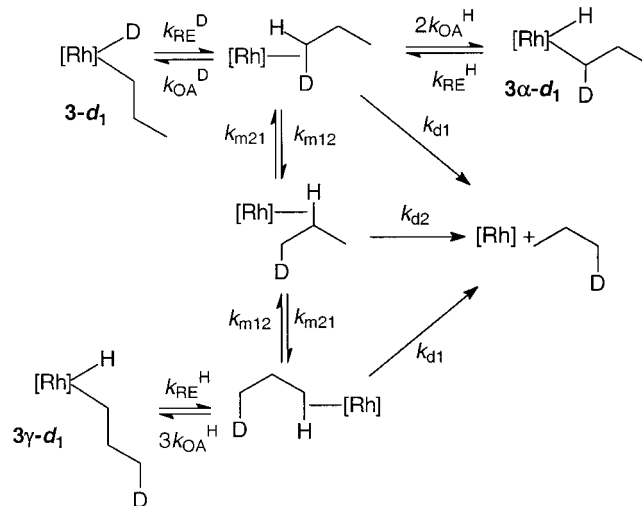
Scheme 10
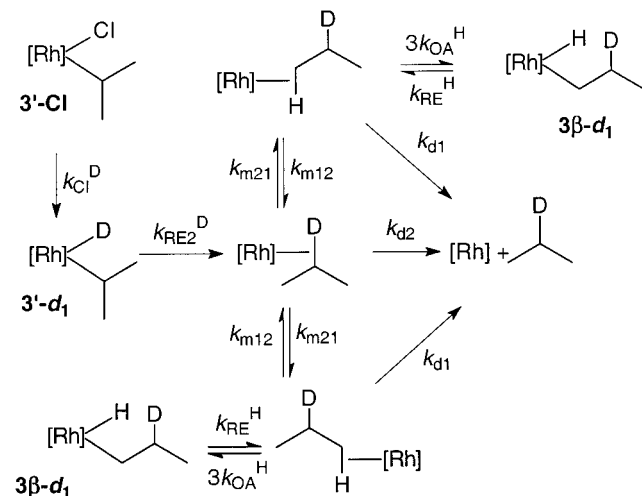
present in the rearrangement of the ethyl deuteride **2-d_1** (Figure 5) than was observed in the reaction of **1-d_1** (Figure 3) due to the increased relative rate of dissociation and the presence of another pathway, namely migration to the "β" position of ethane. Similar migratory behavior was observed for Cp*Rh($^{13}CH_2$-CH_3)D by Bergman and Periana.[7b]

Kinetic Simulation of Alkane Migration: Propane. Kinetic simulation of deuterium scrambling and migration in propyl deuteride complex **3-d_1** proved to be too complex to solve uniquely. Several new rate constants are introduced—primary-to-secondary migration (k_{m12}), secondary-to-primary migration (k_{m21}), and dissociation from a secondary center (k_{d2})—with no additional observed data compared to **2-d_1**. The proposed mechanism for rearrangement is presented in Scheme 9. The irreversible nature of the reductive elimination of propane from isopropyl deuteride complex **3′-d_1** yields a mechanism for rearrangement identical to that for **3-d_1** (Scheme 10), apart from statistical factors, beginning at the isopropyl isomer **3′-d_1** rather than the *n*-propyl isomer. While this additional data might appear to provide the necessary observations to permit a simulation of this kinetic system, the problem still arises that the free energy of the *secondary* σ-propane complex cannot be determined from these experiments. Consequently, the energy of the secondary σ-propane complex was *assumed to be the same* as that of the
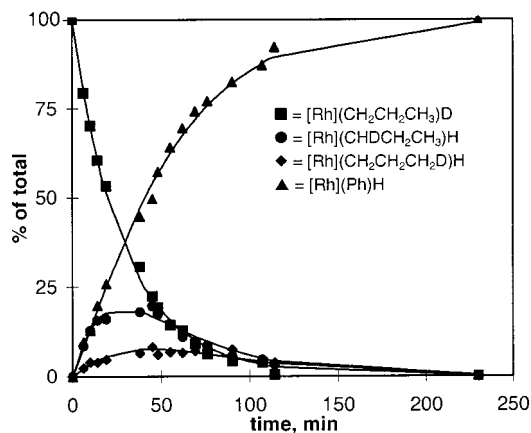
Figure 7. Distribution of species for the rearrangement of **3-d_1** in C_6H_6 at 26 °C. Symbols represent observed data. Solid lines represent simulated data.
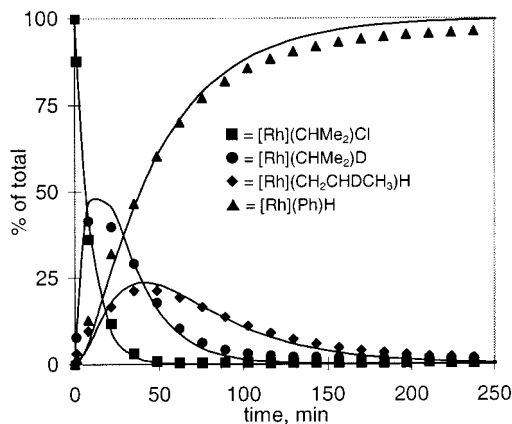
Figure 8. Distribution of species for the rearrangement of **3′-d_1** in C_6H_6 at 26 °C. Symbols represent observed data. Solid lines represent simulated data.

primary σ-propane complex.[24] While few quantitative data are in the literature, this assumption is consistent with the photo-acoustic data measured by Rayner et al., in which $Cr(CO)_5$-(hexane) vs $Cr(CO)_5$(cyclohexane) were found to have similar stabilities.[25]

A *simultaneous* simulation using kinetic data for both reactions with the above constraints allows for determination of all rate constants (5 variables, 8 observables). The comparison of observed and fitted data is shown in Figures 7 and 8. The rate constants obtained from the simultaneous kinetic simulation are presented in Table 4 and presented as a free energy diagram in Figure 9. The simulation again provides information regarding the relative rates of the processes determining the fate of the alkane complex. For the propyl deuteride complex, the relative rate is of the following order: $k_{m21} \approx k_{d2}$; $2k_{OA}^H \approx k_{m12} > k_{d1} > k_{OA}^D \equiv 1.1:1:10:10:3:1$.

The following key points can be drawn from the simulated data. First, when propane is bound in the middle of the alkane as a secondary σ-alkane complex, dissociation and migration to the end of the chain occur at nearly the same rate. Second, when propane is bound at the end of the alkane as a primary

(24) Attempts to simultaneously simulate both the *n*-propyl and isopropyl experiments showed a strong correlation coefficient relating k_{d2} and k_{m21} (0.99999), consistent with the concept that the energy of the secondary alkane complex cannot be determined from these experiments.

(25) Brown, C. E.; Ishikawa, Y.; Hackett, P. A.; Rayner, D. M. *J. Am. Chem. Soc.* **1990**, *112*, 2530. The error limits on the alkane binding strengths make the data of little value for determining the relative binding energies in the present system.

Table 4. Summary of Simulated Rate Constants for Isotopic Scrambling of **3-d_1** and **3′-d_1** in C_6D_6 at 26 °C[a]

rate constant	k, s^{-1}
k_{RE}^H	1.31 (2) $\times 10^{-3}$
k_{RE}^D	**6.2 (2) $\times 10^{-4}$**
k_{OA}^H	2.15 $\times 10^6$
k_{OA}^D	4.33 $\times 10^5$
k_{m12}	**4.3 (9) $\times 10^6$**
k_{m21}	4.3 $\times 10^6$
k_{d1}	**1.26 (47) $\times 10^6$**
k_{d2}	**3.9 (14) $\times 10^6$**
k_{RE2}	**8.1 (5) $\times 10^{-4}$**
k_{Cl}^D	**1.79 (14) $\times 10^{-3}$**

[a] Rate constants that were allowed to vary independently are indicated in bold. Errors are indicated in parentheses at the 95% confidence level (2σ).
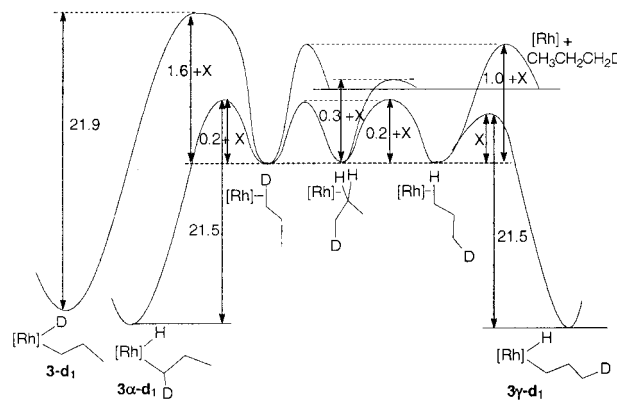
Figure 9. Free energy diagram for the activation of $CH_3CH_2CH_2D$ by [Tp′Rh(CNR)]. Barriers to oxidative addition/reductive elimination from the secondary position are omitted for clarity.

σ-alkane complex, oxidative bond cleavage and migration to the interior of the chain occur at about the same rate; dissociation is ~4−5 times slower, as in ethane.

These results are consistent with the observations made in photolytic activation of propane by **7**, which showed *only* formation of primary activation product **3**.[1m] When bound to the middle of the propane chain, dissociation and migration to the end are much faster than activation. Hence, no secondary activation is observed, leading to the observed kinetic selectivity for the activation of primary C−H bonds.

The equilibrium constant separating a primary σ-alkane complex and a secondary σ-alkane complex cannot be established from the rate constant ratio k_{m12}/k_{m21}, since the assumption that the primary and secondary σ-complexes are at the same energy amounts to an assumption that these rate constants are equal. These experiments only tell about the relative barrier heights seen by each σ-alkane complex separately, as indicated in the free energy diagram in Figure 9. One cannot learn about the absolute free energies of the alkane complexes from these studies. Two studies that address the relative stabilities of various alkane complexes are those using TRIR measurements of alkane binding to $[W(CO)_5]^{11a}$ and fast IR studies looking at competition between Kr and alkane with [Cp*Rh(CO)].[26] These studies generally showed that alkane binding was favored for longer linear alkanes over ethane by 1−2 kcal/mol and that cyclic alkanes bound more tightly than linear alkanes (by ~2 kcal/mol). The nature of the binding of the linear alkanes could not be determined (i.e., primary vs secondary binding).

Kinetic Simulation of Alkane Migration: Butane. A similar kinetic simulation of the rearrangement of *n*-butyl deuteride **4-d_1** (Scheme 11) and *sec*-butyl deuteride **4′-d_1** (Scheme 12) has been possible by varying simultaneously the same five rate constants

Scheme 11
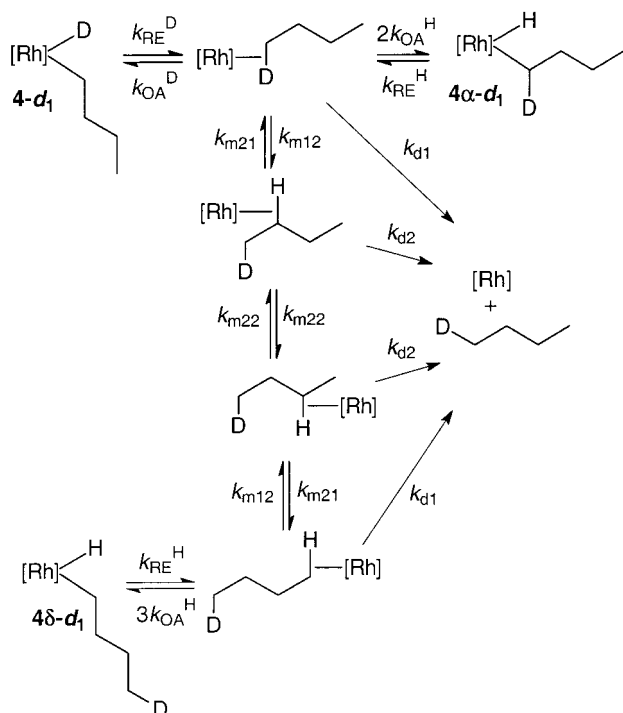
Scheme 12
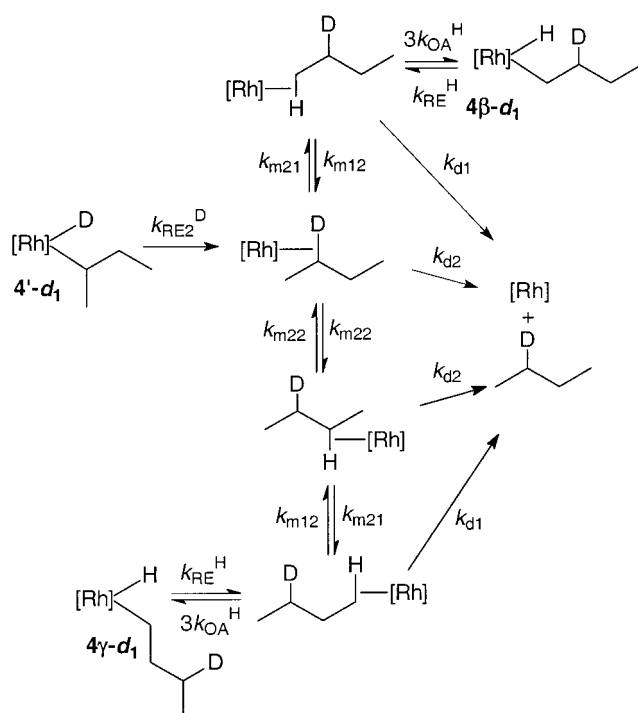
as for **3-d_1** and **3′-d_1**. In addition, the new rate constant for migration from a secondary alkane σ-complex to a secondary alkane σ-complex k_{m22} was also varied, thereby giving the appropriate ratio of the two isomers **4β-d_1** and **4γ-d_1**. The resulting rate constants are listed in Table 5, and the fits are shown in Figures 10 and 11. For the primary alkane σ-complex of butane, oxidative bond cleavage is favored over dissociation by ~6:1 and over 1°−2° migration by ~2:1. For the secondary alkane σ-complex of butane, 2°−2° migration is favored over

(26) McNamara, B. K.; Yeston, J. S.; Bergman, R. G.; Moore, C. B. *J. Am. Chem. Soc.* **1999**, *121*, 6437.

Table 5. Summary of Simulated Rate Constants for Isotopic Scrambling of **4-d_1** and **4′-d_1** in C_6H_6 at 26 °C[a]

rate constant	k, s^{-1}
k_{RE}^{H}	$1.01\,(3) \times 10^{-3}$
k_{RE}^{D}	**$4.82\,(15) \times 10^{-4}$**
k_{OA}^{H}	2.15×10^{6}
k_{OA}^{D}	4.33×10^{5}
k_{m12}	**$3.5\,(8) \times 10^{6}$**
k_{m21}	$3.5\,(8) \times 10^{6}$
k_{m22}	**$1.2\,(6) \times 10^{7}$**
k_{d1}	**$1.08\,(35) \times 10^{6}$**
k_{d2}	**$1.71\,(49) \times 10^{6}$**
k_{RE2}	**$7.67\,(21) \times 10^{-4}$**

[a] Rate constants that were allowed to vary independently are indicated in bold. Errors are indicated in parentheses at the 95% confidence level (2σ).
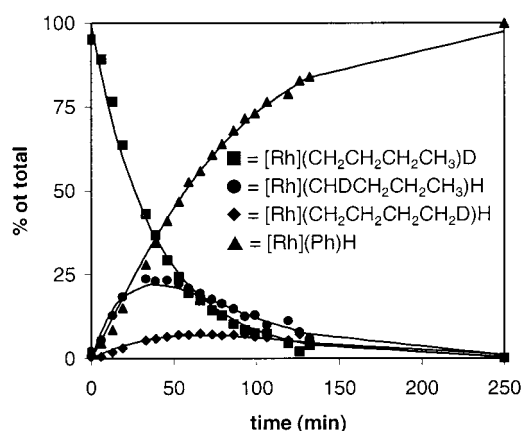
Figure 10. Distribution of species for the rearrangement of **4-d_1** in C_6H_6 at 26 °C. Symbols represent observed data. Solid lines represent simulated data.
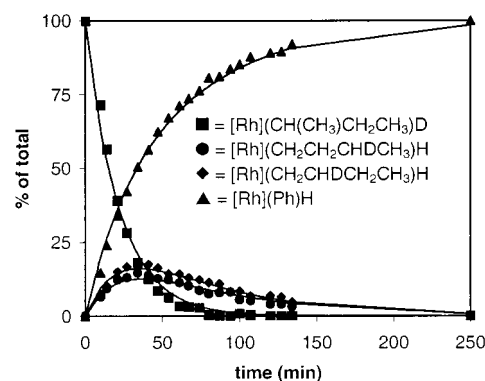
Figure 11. Distribution of species for the rearrangement of **4′-d_1** in C_6H_6 at 26 °C. Symbols represent observed data. Solid lines represent simulated data.

2°−1° migration by ~4:1. Dissociation of the 2° σ-alkane complex occurs about 1.5× faster than the 1° σ-alkane complex.

Kinetic Simulation of Alkane Migration: Pentane and Hexane. The similar isomerizations and alkane loss from pentyl deuteride complex **5-d_1** could be observed, but the small quantity of end-to-end migration made simulation difficult. In the case of hexyl deuteride complex **6-d_1**, the migration to the opposite end of the chain could not be quantified, both because of the small quantity of the complex formed and because of the similarity of the chemical shift of the deuterium in **6φ-d_1** and hexane-d_1. In both cases, however, α-deuterium scrambling was seen to the same extent as in the *n*-propyl and *n*-butyl deuteride species (Figures 12 and 13). The distribution of species in these systems can be simulated using the rate constants obtained from
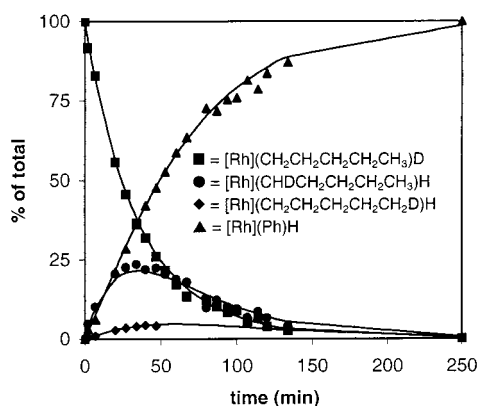
Figure 12. Distribution of species for the rearrangement of **5-d_1** in C_6H_6 at 26 °C. Symbols represent observed data. Solid lines represent simulated data.
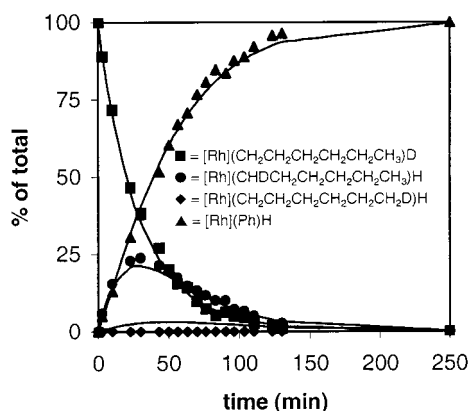
Figure 13. Distribution of species for the rearrangement of **6-d_1** in C_6H_6 at 26 °C. Symbols represent observed data. Solid lines represent simulated data.

the isomerization of butyl deuterides and varying only k_{RE}^D, since no new fundamental rate constants are now needed. The agreement shown in the figures is quite good, again indicating the validity of the kinetic model.

Several assumptions have been made in these detailed kinetic simulations, and further discussion is warranted. First, since the σ-alkane complexes are not directly observed as intermediates an assumption must be made regarding the stability or free energy of these species. The direct observation by Bergman and Harris of the conversion of an alkane σ-complex to an alkyl hydride in the very similar fragment Tp'Rh(CO) offers an excellent estimate for this value. Also, as mentioned earlier, this value ties to the *absolute* values of the "fast" processes (k_{OA}^H, k_{OA}^D, k_m, k_d), but does not affect their *relative* values. As the latter are what are needed to determine selectivities, the conclusions drawn here are independent of the value used for k_{OA}^H!

Second, in dealing with the problems presented by the isotope effects introduced as a result of using deuterium to monitor the rearrangements of the complexes, we used the reductive elimination rates for the isopropyl hydride vs the isopropyl deuteride complex to obtain $k_{RE}^H/k_{RE}^D = 2.1$ for the isotope effect on alkane reductive bond formation to give an alkane σ-complex. While the absolute rate constants for reductive bond formation from primary alkyl hydride and alkyl deuteride complexes are likely to be different, it is reasonable to assume that the *ratio* of these rates (i.e. the isotope effect) is of similar size. It is this assumption that allows one to solve the methyl deuteride simulation.

Third, to solve the ethyl deuteride scrambling simulation it is also assumed that the isotope effect on oxidative bond cleavage is the same in the formation of an *n*-alkyl hydride complex as it is in the formation of the methyl hydride complex ($k_{OA}^H/k_{OA}^D = 5.0$). This is a reasonable assumption in that in either case the factors that make reaction of one isotope favored over another (zero point energies, bending energies) are similar in this series of compounds. The independent measurement of k_{OA}^H/k_{OA}^D with CH_2D_2 confirms that this assumption is reasonable.

Finally, we assumed in our treatment that equilibration between the various C−H and C−D bonds on a given carbon center in an alkane σ-complex is rapid, and that these species are equally accessible. In the σ-cyclopentane complex described by Ball, the metal was believed to rapidly migrate from one C−H to the other within the same methylene unit, although an η^2-H,H binding geometry could not be ruled out.[10] In studies of an agostic methyl group by Shapley in $Os_3(CH_2D)(CO)_{11}$, migration between C−H and C−D was fast on the NMR time scale and a preference for binding C−H vs C−D was only 1.25.[27] More to the point, in a recent study by Etienne, an intramolecular agostic equilibrium isotope effect was directly measured to be 1.2 in a niobium ethyl derivative.[28] In the present system, a similar slight preference for binding C−H vs C−D bonds is also likely to be present. This equilibrium effect between η^2-C,H and η^2-C,D alkane σ-complexes is of small (but probably real) importance in the kinetic treatment used here. One alternate way to view this effect is to say that all of the k_{OA}^D values obtained here include in them an equilibrium contribution to the rate constant, estimated to contribute ∼25% of the kinetic isotope effect. In the absence of relevant data here, and considering the small magnitude of this correction, the present treatment using the assumption of equal access to C−H and C−D bonds was adopted. One contrary report suggests that intermolecular equilibrium isotope effects favor binding of C−D bonds, but in contrast to the present system the alkane in this example was weakly bound and freely exchanged with other alkanes in the krypton solvent prior to oxidative bond cleavage.[3]

It is also worthwhile to compare the quantitative results obtained here with the qualitative results obtained by Flood on the deuterium scrambling in [CnRh(L)RD]$^+$ complexes (L = P(OMe)$_3$, Cn = 1,4,7-triazacyclononane).[14] In his case, butyl, hexyl, and even decyl groups were observed to undergo complete equilibration of the deuterium into the α-position at 5 °C. The observed (statistically corrected) equilibrium constant was 1.7, favoring deuterium on carbon, and is *exactly* what was observed in the present system with CH_2D_2 as the substrate (eq 8). Furthermore, upon heating to 40 °C Flood observed subtantial quantities of deuterium migration into the terminal methyl group of even the *n*-decyl ligand, indicating that the metal is capable of migrating down a 10-carbon chain without dissociating. Clearly, the [CnRh(L)]$^+$ fragment binds alkanes more tightly than [Tp'Rh(L)], perhaps due to its positive charge.

Conclusions

The isotopic scrambling and rearrangement of complexes of the type Tp'Rh(CNR)(R)(H/D) has been shown to proceed intramolecularly with alkane σ-complexes as intermediates. Rearrangement of secondary alkyl hydrides to their more stable primary alkyl hydride isomers was observed. Scrambling of

(27) Calvert, R. B.; Shapley, J. R. *J. Am. Chem. Soc.* **1978**, *100*, 7726.
(28) Jaffart, J.; Mathieu, R.; Etienne, M.; McGrady, J. E.; Eisenstein, O.; Maseras, F. *Chem. Commun.* **1998**, 2011.
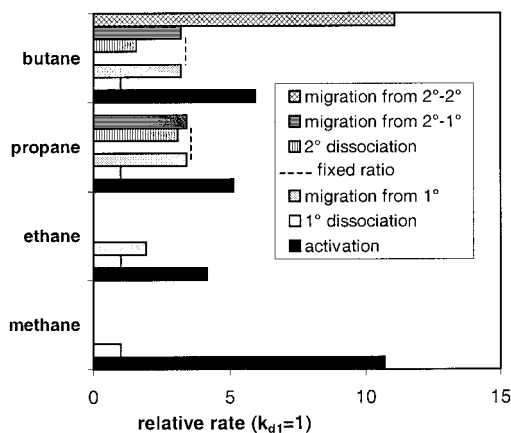
Figure 14. Bar graph showing relative rates of reactions of σ-alkane complexes. For propane and butane, the processes for the primary and secondary σ-alkane complexes are separated.

deuterium label into both the α-position and terminal methyl group was observed in linear alkyl deuteride complexes **2-d_1** to **6-d_1**. Relative rates of dissociation, migration, and bond activation from alkane complexes have been elucidated through kinetic simulation, allowing several general conclusions to be drawn. For methane, C−H bond activation is strongly favored over dissociation of methane from the metal−methane σ-complex. For ethane−hexane, activation of the terminal C−H bond of the alkane is favored over both dissociation and migration to the β position of the σ-alkane complex.

Propane and the higher alkanes offer an opportunity to learn about a number of competitive processes available to alkane complexes, as alluded to in the discussion of eqs 3−5. The relative rates of these processes available to alkane complexes of methane, ethane, propane, and butane are shown schematically in Figure 14. Due to the ability to obtain only relative rates for a given alkane complex, these rates cannot be compared from one substrate to another, or even from one alkane σ-complex to another.

The following general conclusions can be made about these processes for the fragment [Tp′Rh(CNR)] interacting with a linear alkane: (1) C−H bond activation is favored over dissociation of alkane in a primary alkane σ-complex by a factor of ∼five, (2) primary-to-secondary and secondary-to-primary migrations are faster than dissociation from their respective alkane σ-complexes by a factor of 2−3 while secondary-to-secondary migration is about 7× faster than dissociation, (3) C−H activation is the fastest process in primary alkane complexes, but the slowest in secondary alkane complexes (it is not even observed in the latter case, unless no other type of bond is available (e.g. cycloalkanes)), and (4) in a secondary alkane σ-complex, secondary-to-secondary migration is about 3× faster than secondary-to-primary migration, giving rise to the effect of rapid migration down a linear chain.

Inverse isotope effects on alkane loss from an alkyl hydride vs an alkyl deuteride complex have been shown to be the result of an inverse preequilibrium isotope effect, produced by two different but normal isotope effects in the reductive bond formation/oxidative bond cleavage preequilibrium steps.

Experimental Section

General Considerations. All manipulations were performed under an N_2 atmosphere, either on a high-vacuum line using modified Schlenk techniques or in a Vacuum Atmospheres Corporation Glovebox. Tetrahydrofuran and toluene were distilled from dark purple solutions of benzophenone ketyl. Alkane solvents were made olefin-free by

stirring over H_2SO_4, washing with aqueous $KMnO_4$ and water, and distilling from dark purple solutions of tetraglyme/benzophenone ketyl. Tetrahydrofuran-d_8, benzene-d_6, and methane-d_2 were purchased from Cambridge Isotope Lab. The liquids were distilled under vacuum from dark purple solutions of benzophenone ketyl and stored in ampules with Teflon sealed vacuum line adaptors. The preparations of KTp′,[29] Tp′Rh(L)Cl$_2$,[16a] Tp′Rh(L)(Me)Cl,[16a] Tp′Rh(L)(*n*-Pr)Cl,[16a] Tp′Rh(L)-(*i*-Pr)Cl,[16a] Tp′Rh(L)(*n*-Pr)H[1m], Tp′Rh(L)(*n*-pentyl)Cl[1m], Tp′Rh(L)-(*n*-pentyl)H,[1m] Tp′Rh(L)(η^2-PhN=C=NCH$_2$C(CH$_3$)$_3$),[30] and neopentylisocyanide (L)[31] have been previously reported. We have additionally noted that in the preparation of Tp′Rh(CNneopentyl)Cl$_2$, the *fac*-isomer of RhCl$_3$(CH$_3$CN)$_3$ must be used. Caution must be taken during the preparation of this intermediate from RhCl$_3$·3H$_2$O (do not heat) or the unreactive *mer*-isomer can be formed. The zirconium reagents [Cp$_2$-ZrH$_2$]$_2$ and [Cp$_2$ZrD$_2$]$_2$ were prepared according to literature methods.[32] All Grignards with the exception of *n*-pentylmagnesium chloride and *n*-hexylmagnesium chloride were purchased from Aldrich Chemical Co. Hexafluorobenzene (C$_6$F$_6$) was purchased from the Aldrich Chemical Co, dried over 4 Å Linde molecular sieves for 24 h, degassed using three freeze−pump−thaw cycles, and stored in the dri-lab.

All NMR spectra were recorded on a Bruker AMX400 (^{1}H, ^{2}H, ^{11}B, ^{13}C). All ^{1}H and ^{2}H chemical shifts are reported in ppm (δ) relative to tetramethylsilane and referenced using chemical shifts of residual solvent resonances (benzene-d_6, δ 7.15). ^{11}B NMR spectra were referenced to external BF$_3$·OEt$_2$ (δ 0.0). All temperatures for kinetic experiments were calibrated relative to the chemical shift differences in the NMR spectra of neat ethylene glycol. Accurate temperature control ($\pm$0.1 °C) was maintained using a Bruker BVT-3000 VT control unit. Resealable NMR tubes with Teflon valves were purchased from the Brunfeldt Co. Infrared spectra were recorded on a Mattson Instruments 6020 Galaxy Series FTIR and processed with First:Acquire v1.52 software. Analyses were obtained from Desert Analytics. A Siemens SMART system with a CCD area detector was used for X-ray structure determination.

Preparation of Tp′Rh(L)(Et)Cl, 2-Cl. Tp′Rh(L)Cl$_2$ (155 mg, 0.27 mmol) was placed in a 50 mL round-bottom flask with a Teflon coated stir bar. Addition of 25 mL of THF resulted in a yellow orange solution. Ethylmagnesium chloride (0.20 mL, 0.40 mmol, 1.5 equiv) was added dropwise to the stirring solution over 5 min and the resulting brown solution stirred for 15 min. Excess Grignard reagent was quenched with a saturated solution of NH$_4$Cl(aq) until all had reacted to give a clear solution. The pale yellow solution was filtered through glass wool and solvent removed under vacuum. Purification was by preparative TLC using hexanes−THF (4:1, *v/v*) as the mobile phase. Recrystallization at −20 °C from a CH$_2$Cl$_2$ solution layered with hexanes yielded 97 mg (0.17 mmol, 64%) of bright yellow X-ray quality crystals. NMR data for **2-Cl**: ^{1}H NMR (C$_6$D$_6$) δ 5.712 (s, 1 H, pz*H*), 5.604 (s, 1 H, pz*H*), 5.566 (s, 1H, pz*H*), 3.613 (m, C*H*HCH$_3$, 1 H), 3.385 (m, C*H*HCH$_3$, 1 H), 2.981 (s, 3H, pzC*H$_3$*), 2.775 (s, 3H, pzC*H$_3$*), 2.656 (AB$_q$, 2H, NCH$_2$), 2.343 (s, 3H, pzC*H$_3$*), 2.230 (s, 3H, pzC*H$_3$*), 2.154 (s, 3H, pzC*H$_3$*), 2.095 (s, 3H, pzC*H$_3$*), 1.355 (t, J_{HH} = 7.6 Hz, 3H, CH$_2$C*H$_3$*), 0.716 (s, 9H, CH$_2$C(C*H$_3$*)$_3$). ^{13}C{^{1}H} NMR (C$_6$D$_6$) δ 155.70, 153.76, 153.35, 146.93, 145.41, 145.17 (s, pzC$_q$), 111.15, 110.33, 109.26 (s, pzCH), 58.79 (s, NCH$_2$), 34.54 (s, *C*(CH$_3$)$_3$), 29.23 (s, C(*C*H$_3$)$_3$), 21.48 (s, Rh*C*H$_2$CH$_3$), 17.25, 15.63, 15.39, 14.92 (s, pzCH$_3$), 13.98 (d, J_{RhH} = 18.7 Hz, RhCH$_2$*C*H$_3$). IR (THF, cm^{-1}) 2521 (w, B−H), 2203 (s, CNR). Anal. Calcd for C$_{23}$H$_{38}$BClN$_7$Rh: C, 49.18; H, 6.82; N, 17.45. Found: C, 48.54; H, 6.80; N, 17.46.

Preparation of Tp′Rh(L)(*n*-Bu)Cl, 4-Cl. Synthesis of **4-Cl** was identical to that of **2-Cl** except that 190 mg of Tp′Rh(L)Cl$_2$ (0.36 mmol) and 0.27 mL of 2.0 M *n*-butylmagnesium chloride (0.54 mmol, 1.5 equiv) were used. Workup and recrystallization of **4-Cl** were identical to that of **2-Cl**. Yield: 86 mg (0.146 mmol, 41%). NMR data for **4**: ^{1}H NMR (C$_6$D$_6$) δ 5.699 (s, 1 H, pz*H*), 5.608 (s, 1 H, pz*H*), 5.556 (s, 1H, pz*H*), 3.442 (m, C*H*HCH$_2$CH$_3$, 1 H), 3.290 (m, C*H*HCH$_2$-CH$_3$, 1 H), 2.969 (s, 3H, pzC*H$_3$*), 2.776 (s, 3H, pzC*H$_3$*), 2.642 (AB$_q$,

(29) Trofimenko, S. *Inorg. Synth.* **1970**, *12*, 99.
(30) Hessel, E. T.; Jones, W. D. *J. Am. Chem. Soc.* **1992**, *114*, 6087.
(31) Schuster, R. E. *Organic Synthesis*; Wiley: New York, 1973; Collect. Vol. V, p 772.
(32) Shriver, D. F. *Inorg. Synth.* **1979**, *19*, 223.

2H, NCH₂), 2.360 (s, 3H, pzCH₃), 2.220 (s, 3H, pzCH₃), 2.148 (s, 3H, pzCH₃), 2.086 (s, 3H, pzCH₃), 1.987 (m, CH₂CHHCH₂CH₃, 1 H), 1.762 (m, CH₂CHHCH₂CH₃, 1 H), 1.690 (m, CH₂CH₂CH₂CH₃, 2 H), 1.041 (t, J_{HH} = 7.2 Hz, 3H, RhCH₂CH₂CH₂CH₃), 0.709 (s, 9H, CH₂C(CH₃)₃). ¹³C{¹H} NMR (C₆D₆) δ 153.13, 151.17, 150.83, 144.38, 142.84, 142.59 (s, pzC_q), 108.58, 107.81, 106.70 (s, pzCH), 56.27 (s, NCH2), 36.61 (s, RhCH₂CH₂CH₂CH₃), 32.01 (s, C(CH₃)₃), 26.68 (s, C(CH₃)₃), 26.18 (s, RhCH₂CH₂CH₂CH₃), 18.37 (d, J_{RhH} = 19.0 Hz, RhCH₂CH₂CH₂-CH₃), 14.72, (s, pzCH₃), 14.69 (s, RhCH₂CH₂CH₂CH₃), 14.52, 13.05, 12.83, 12.36 (s, pzCH₃). IR (THF, cm⁻¹) 2524 (w, B−H), 2205 (s, CNR). Anal. Calcd for C₂₅H₄₂BClN₇·CH₂Cl₂: C, 46.3; H, 6.57; N, 14.53. Found: C, 45.21; H, 6.37; N, 13.62.

Preparation of Tp′Rh(L)(n-pentyl)Cl, 5-Cl. Synthesis of **5**-Cl was identical to that of **2**-Cl except that 238 mg of Tp′Rh(L)Cl₂ (0.41 mmol) and 1.50 mL of 0.30 M n-hexylmagnesium chloride (0.450 mmol, 1.1 equiv) were used. Workup and recrystallization of **5**-Cl were identical to that of **2**-Cl. Yield: 64.7 mg (0.107 mmol, 26.1%).

Preparation of Tp′Rh(L)(n-hexyl)Cl, 6-Cl. Synthesis of **6**-Cl was identical to that of **2**-Cl except that 274 mg of Tp′Rh(L)Cl₂ (0.48 mmol) and 1.50 mL of 0.37 M n-hexylmagnesium chloride (0.555 mmol, 1.2 equiv) were used. Workup and recrystallization of **6**-Cl were identical to that of **2**-Cl. Yield: 104 mg (0.168 mmol, 34.7%). NMR data for **6**-Cl: ¹H NMR (C₆D₆): δ 5.699 (s, 1 H, pzH), 5.608 (s, 1 H, pzH), 5.556 (s, 1H, pzH), 3.442 (m, CHHCH₂CH₂CH₃, 1 H), 3.290 (m, CHHCH₂CH₂CH₃, 1 H), 2.969 (s, 3H, pzCH₃), 2.776 (s, 3H, pzCH₃), 2.642 (AB_q, 2H, NCH₂), 2.360 (s, 3H, pzCH₃), 2.220 (s, 3H, pzCH₃), 2.148 (s, 3H, pzCH₃), 2.086 (s, 3H, pzCH₃), 1.987 (m, CH₂CHHCH₂-CH₃, 1 H), 1.762 (m, CH₂CHHCH₂CH₃, 1 H), 1.690 (m, CH₂CH₂CH₂-CH₃, 2 H), 1.041 (t, J_{HH} = 7.2 Hz, 3H, RhCH₂CH₂CH₂CH₃), 0.709 (s, 9H, CH₂C(CH₃)₃). ¹³C{¹H} NMR (C₆D₆): δ 153.2, 151.2, 150.8, 144.4, 142.9, 142.6 (s, pzC_q), 108.6, 107.8, 106.7 (s, pzCH), 56.3 (s, NCH2), 34.3, 33.2, 32.5 (s, RhCH₂(CH₂)₄CH₃), 32.0 (s, C(CH₃)₃), 26.7 (s, C(CH₃)₃), 23.4 (s, RhCH₂(CH₂)₃CH₂CH₃), 18.8 (d, J_{RhH} = 19.0 Hz, RhCH₂(CH₂)₄CH₃), 14.7, 14.4, 13.1, 12.8, 12.3 (s, pzCH₃). IR (THF, cm⁻¹): 2521 (w, B−H), 2205 (s, CNR). Anal. Calcd for C₂₇H₄₆BClN₇-Rh: C, 52.49; H, 7.50; N, 15.87. Found: C, 52.94; H, 7.59; N, 15.47.

Preparation of Tp′Rh(L)(sec-butyl)Cl, 4′-Cl. Synthesis of **4′**-Cl was identical to that of **2**-Cl except that 124 mg of Tp′Rh(L)Cl₂ (0.23 mmol) and 0.23 mL of 2.0 M sec-butylmagnesium chloride (0.46 mmol, 2 equiv) were used. Workup and recrystallization of **4′**-Cl were identical to that of **2**-Cl. Yield: 14.4 mg (0.024 mmol, 10.5%). Recrystallization from methanol at −20 °C allows for partial crystallization of one stereoisomer of **4′**-Cl. NMR data for **4′**-Cl: ¹H NMR (C₆D₆) δ 5.695, 5.686 (s, 1 H, pzH), 5.638 (bs, 2 H, pzH), 5.566, 5.560 (s, 1H, pzH), 4.89 (bm, 1H, RhCH(CH₂CH₃)CH₃), 3.046, 3.031 (s, 3H, pzCH₃), 2.775, 2.772 (s, 3H, pzCH₃), 2.672, 2.660 (AB_q, 2H, NCH₂), 2.401, 2.370 (s, 3H, pzCH₃), 2.216, 2.212 (s, 3H, pzCH₃), 2.184, 2.172 (s, 3H, pzCH₃), 2.118, 2.108 (s, 3H, pzCH₃), 1.940 (bm, 4H, RhCH(CH₂-CH₃)CH₃), 1.049 (bt, J_{HH} = 8.4 Hz, 6H, RhCH(CH₂CH₃)CH₃), 0.707, 0.694 (s, 9H, CH₂C(CH₃)₃). ¹³C{¹H} NMR (C₆D₆) δ 153.2, 151.2, 150.8, 144.4, 142.9, 142.6 (s, pzC_q), 108.6, 107.8, 106.7 (s, pzCH), 56.3 (s, NCH2), 34.3, 33.2, 32.5 (s, RhCH₂(CH₂)₄CH₃), 32.0 (s, C(CH₃)₃), 26.7 (s, C(CH₃)₃), 23.4 (s, RhCH₂(CH₂)₃CH₂CH₃), 18.8 (d, J_{RhH} = 19.0 Hz, RhCH₂(CH₂)₄CH₃), 14.7, 14.4, 13.1, 12.8, 12.3 (s, pzCH₃). IR (THF, cm⁻¹) 2521 (w, B−H), 2205 (s, CNR).

Preparation of Tp′Rh(L)(R)H. To a resealable NMR tube was added 7.8 mg of ethyl derivative **2**-Cl (0.014 mmol) and 12.3 mg (0.027 mmol) of [Cp₂ZrH₂]₂. Benzene-d₆ (0.55 mL) was added via syringe. The reaction mixture was shaken vigorously for 1 min, with complete conversion to **2** by ¹H NMR spectroscopy. The unreacted [Cp₂ZrH₂]₂ and Cp₂ZrCl₂ precipitate to the bottom of the sample. The reaction is general and was used to form hydrides **1−4′**. Data for **3**, **5**, and **3′** were reported earlier. For **2**: ¹H NMR (C₆D₆) δ 5.825 (s, 1 H, pzH), 5.660 (s, 1 H, pzH), 5.642 (s, 1H, pzH), 2.628 (AB_q, 2H, NCH₂), 2.570 (s, 3H, pzCH₃), 2.558 (s, 3H, pzCH₃), 2.354 (s, 3H, pzCH₃), 2.269 (s, 3H, pzCH₃), 2.194 (s, 3H, pzCH₃), 2.170 (s, 3H, pzCH₃), 1.619 (t, J_{HH} = 7.6 Hz, 3H, CH₂CH₃), 0.658 (s, 9H, CH₂C(CH₃)₃), −14.936 (d, J_{RhH} = 24.8 Hz, 1H RhH). For **4**: ¹H NMR (C₆D₆) δ 5.816 (s, 1 H, pzH), 5.646 (s, 1 H, pzH), 5.627 (s, 1H, pzH), 2.667 (AB_q, 2H, NCH₂), 2.572 (s, 3H, pzCH₃), 2.561 (s, 3H, pzCH₃), 2.368 (s, 3H, pzCH₃), 2.267 (s, 3H, pzCH₃), 2.206 (s, 3H, pzCH₃), 2.183 (s, 3H, pzCH₃), 1.931

(m, 2H, RhCH₂CH₂CH₂CH₃), 1.669 (m, 2H, RhCH₂CH₂CH₂CH₃), 1.107 (t, J_{HH} = 7.6 Hz, 3H, RhCH₂CH₂CH₂CH₃), 0.658 (s, 9H, CH₂C(CH₃)₃), −14.993 (d, J_{RhH} = 24.8 Hz, 1H RhH). For **6**: ¹H NMR (C₆D₆) δ 5.808 (s, 1 H, pzH), 5.637 (s, 1 H, pzH), 5.620 (s, 1H, pzH), 2.652 (AB_q, 2H, NCH₂), 2.576 (s, 3H, pzCH₃), 2.564 (s, 3H, pzCH₃), 2.360 (s, 3H, pzCH₃), 2.274 (s, 3H, pzCH₃), 2.194 (s, 3H, pzCH₃), 2.172 (s, 3H, pzCH₃), 1.927 (m, 2H, RhCH₂CH₂CH₂CH₂CH₃), 1.636 (m, 2H, RhCH₂CH₂CH₂CH₂CH₃), 1.466 (m, 2H, RhCH₂CH₂CH₂CH₂-CH₂CH₃), 1.384 (m, 2H, RhCH₂CH₂CH₂CH₂CH₂CH₃), 0.904 (t, J_{HH} = 7.6 Hz, 3H, RhCH₂CH₂CH₂CH₂CH₂CH₃), 0.648 (s, 9H, CH₂C-(CH₃)₃), −14.928 (d, J_{RhH} = 24.8 Hz, 1H RhH). For **4′**: ¹H NMR (C₆D₆) δ 5.818 (s, 2 H, pzH), 5.636 (s, 2 H, pzH), 5.564 (s, 1H, pzH), 5.558 (s, 1H, pzH), 2.694 (AB_q, 4H, NCH₂), 2.603 (s, 3H, pzCH₃), 2.597 (s, 3H, pzCH₃), 2.438 (s, 6H, pzCH₃), 2.363 (s, 3H, pzCH₃), 2.320 (s, 3H, pzCH₃), 2.302 (s, 6H, pzCH₃), 2.248 (s, 6H, pzCH₃), 2.194 (s, 6H, pzCH₃), 1.216 (t, J_{HH} = 6.8 Hz, 3H, CH(CH₃)CH₂CH₃), 1.190 (t, J_{HH} = 7.2 Hz, 3H, CH(CH₃)CH₂CH₃), 0.658 (s, 9H, CH₂C(CH₃)₃), −15.294 (d, J_{RhH} = 24.8 Hz, 1H RhH), −15.302 (d, J_{RhH} = 25.2 Hz, 1H RhH).

Kinetics of Elimination of Alkane from Tp′Rh(L)(R)H. Generation of rhodium alkyl hydride complexes was accomplished by the general method outlined above, with 1 μL of dimethoxyethane (DME) added as an internal standard. The reductive elimination of alkane from **1−6** was monitored by ¹H NMR spectroscopy in C₆D₆ at 26 °C. For kinetic analysis neopentyl isocyanide resonances for both Tp′Rh(L)-(C₆D₅)D and alkyl hydride were integrated relative to DME at regular intervals. Data analysis was carried out using Microsoft Excel (see Supporting Information).

Preparation of Tp′Rh(L)(R)D. To a resealable NMR tube was added 8.0 mg of ethyl derivative **2**-Cl (0.014 mmol) and 22.3 mg (0.049 mmol) of [Cp₂ZrD₂]₂. Benzene (0.55 mL) and benzene-d₆ (1 μL) were added via syringe. The reaction mixture was shaken vigorously for 1 min and placed into a pre-shimmed probe. The reaction is general and was used to form the isotopomers **1-d₁** to **4′-d₁**. For **2-d₁**: {¹H}²H NMR (C₆H₆) δ 2.528 (RhCHDCH₃), 2.180 (RhCH₂CH₂D), −14.825. **3-d₁**: {¹H}²H NMR (C₆H₆) δ 2.339, 2.048 (RhCHDCH₂CH₃), 1.313 (RhCH₂-CH₂CH₂D), −14.791 (RhD). **4-d₁**: {¹H}²H NMR (C₆H₆) δ 2.438, 2.082 (RhCHD(CH₂)₂CH₃), 1.937 (RhCH₂CHDCH₂CH₃), 1.656 (Rh(CH₂)₂-CHDCH₃), 1.126 (RhCH₂(CH₂)₂CH₂D), −14.782 (RhD). **5-d₁**: {¹H}²H NMR (C₆H₆) δ 2.366, 2.056 (RhCHD(CH₂)₃CH₃), 1.008 (RhCH₂(CH₂)₃-CH₂D), −14.810 (RhD). **6-d₁**: {¹H}²H NMR (C₆H₆) δ 2.332, 2.029 (RhCHD(CH₂)₄CH₃), 14.829 (RhD). **3′-d₁**: {¹H}²H NMR (C₆H₆) δ −15.122 (RhD). **4′-d₁**: {¹H}²H NMR (C₆H₆) δ −15.218 (RhD).

Kinetics of Isomerization of Tp′Rh(L)(R)D. Generation of rhodium alkyl deuteride complexes was accomplished by the general method outlined above, with 1 μL of benzene-d₆ added as an internal standard. Isomerization and migration of the deuterium label in **1−4′** was monitored by {¹H}²H NMR spectroscopy in C₆H₆ at 26 °C. For kinetic analysis all signals were integrated relative to C₆D₆ at regular intervals (see Figure 2). The relative amounts of each species were measured by calculating the ratio of the integral value of one species to the sum of the integral value for all species (all species contain one deuterium). Kinetic simulation was carried out using KINSIM/FITSIM (see Supporting Information). Agreement is generally good, with the largest deviations being observed for the lighter hydrocarbons (methane, ethane, propane) at longer reaction times due to their volatility.

Determination of Isotope Effects on Oxidative Addition. Tp′Rh-(L)(η²-PhN═C═NCH₂C(CH₃)₃) (6 mg, 0.009 mmol) was placed in a resealable NMR tube. C₆F₆ (0.6 mL) was added via syringe. The resulting bright yellow solution was degassed three times. The vacuum manifold was filled with 0.105 atm of CH₂D₂ (2.0 mmol). CH₂D₂ was condensed into the NMR tube and carefully thawed. (CAUTION: Extremely high pressure!) The sample was photolyzed for 6 min at 6 °C until the bright yellow solution became completely bleached. The sample was placed in a −10 °C methanol/water bath and the pressure released. The NMR probe (at 9 °C) was shimmed with a C₆D₆ sample of Tp′Rh(C₆D₅)D of similar concentration and solvent height. {²H}¹H NMR spectra were acquired unlocked. The methyl signals of the two C−X bond activation products were integrated relative to the single neopentyl isocyanide resonance for **1-d₂**. This ratio was used to

7270 *J. Am. Chem. Soc., Vol. 123, No. 30, 2001*

Northcutt et al.

determine the kinetic isotope effect. For **1a**-*d*$_2$: {^{2}H}^{1}H NMR (C$_6$F$_6$) δ 0.091 downfield from CH$_2$D$_2$. For **1b**-*d*$_2$: {^{2}H}^{1}H NMR (C$_6$F$_6$) δ 0.195 downfield from CH$_2$D$_2$.

Supporting Information Available: Tables of kinetic fits and experimental details of the X-ray structural determinations of **2-Cl** and **6-Cl** (PDF). This material is available free of charge via the Internet at http://pubs.acs.org.

JA003944X